A photoionized Herbig-Haro object in the Orion nebula

K. P. M. Blagrave and P. G. Martin

Department of Astronomy and Astrophysics and Canadian Institute for Theoretical Astrophysics, University of Toronto, 60 St. George Street, Toronto, ON M5S 3H8, Canada

blagrave@cita.utoronto.ca, pgmartin@cita.utoronto.ca

and

J. A. Baldwin

Physics and Astronomy Department, 3270 Biomedical Physical Sciences Building, Michigan State University, East Lansing, MI 48824

baldwin@pa.msu.edu

ABSTRACT

The spectra of Herbig Haro objects are usually characteristic of ionization and excitation in shock-heated gas, whether an internal shock in an unsteady outflow or a bow shock interface with the interstellar medium. We examine the eastern-most shock – the leading optically visible shock – of a Herbig Haro outflow (HH 529) seen projected on the face of the Orion Nebula, using deep optical echelle spectroscopy, showing that the spectrum of this gas is consistent with photoionization by θ^1 Ori C. By modeling the emission lines, we determine a gas-phase abundance of Fe which is consistent with the depleted (relative to solar) abundance found in the Orion nebula – evidence for the presence of dust in the nebula and therefore in the Herbig Haro outflow. The spectrum also allows for the calculation of temperature fluctuations, t^2, in the nebula and the shock. These fluctuations have been used to explain discrepancies between abundances obtained from recombination lines versus those obtained from collisionally-excited lines, although to date there has not been a robust theory for how such large fluctuations ($t^2 > 0.02$) can exist.

Subject headings: H II regions—ISM: Herbig-Haro objects—dust

1. Introduction

Star-forming regions – such as the Orion Nebula – are home to various phenomena associated with the early stages of stellar evolution. Some of the more prominent features in the visible part of the spectrum are the arcs associated with gas flows known as Herbig Haro (HH) flows (Reipurth & Bally 2001). Many of these flows have been identified in the Orion Nebula and have had both their radial (Doi et al. 2004) and tangential (Doi et al. 2002) velocities measured. The origins of these flows have in a few cases been associated with IR sources embedded within the Orion Molecular Cloud 1 South (OMC-1S) (Doi et al. 2002). However, there are many flows that have not been paired with any source (X-ray, radio, or near-IR) – including HH 529 (O'Dell & Doi 2003). This flow contains at least three curved shocks which appear in [O III] WFPC2 images (O'Dell & Wong 1996) and extend approximately 36″ from the centre of the inferred source of the optical outflow (OOS) at α, δ (J2000) = $5^{\rm h}35^{\rm m}14\overset{\rm s}{.}56$,$-5^{\rm o}23'54''$(O'Dell & Doi 2003; Doi et al. 2004).[1] This is 0.08 pc in the plane of sky given a distance to the nebula of 460 pc (Bally et al. (2000), hereafter BOM).

The radial (line-of-sight) velocity is -44 km s^{-1} (Doi et al. 2004). This radial velocity is quoted as "systemic" – relative to the [O III] nebular component, which itself has a heliocentric velocity of $+18 \pm 2$ km s^{-1} (Doi et al. 2004). Coupling this with the heliocentric radial velocity of the PDR (+28 km s^{-1}, Goudis (1982)), we obtain a radial velocity relative to the source embedded within OMC-1: -54 km s^{-1}. The average proper motion velocity is 54 km s^{-1} (Doi et al. 2004) which leads to a total velocity of 76 km s^{-1} (with respect to OMC-1S) at an angle of 45° out of the plane of the sky.

Using this geometry, a distance from the embedded source to the leading edge of the eastern-most shock can be calculated: 0.12 pc ($36'' \times \sqrt{2}$). Assuming that the source lies within OMC-1S and that θ^1 Ori C is itself ~ 0.25 pc from the main ionization front (Wen & O'Dell 1995; O'Dell 2001a), this would place the HH 529 system on the far side (i.e., further from the observer) of θ^1 Ori C. It is remarkable that the flow has emerged from the cloud

[1] In addition to HH 529, many other HH flows (HH 269, HH 202 and HH 203/204) appear to originate in the OOS region – supplying ample evidence for OOS housing HH flow driver(s). Smith et al. (2004) have detected an infrared source (IR source 2 in their Table 2; α, δ = $5^{\rm h}35^{\rm m}14\overset{\rm s}{.}40$,$-5^{\rm o}23'51\overset{''}{.}0$) which lies within 3″ of the predicted location of the OOS. Zapata et al. (2004) have also observed this source at 1.3cm. Within the OOS region, Bally et al. (2000) have identified another near-IR source ('s' in their Fig. 20) which was concurrently labelled HC209 (Hillenbrand & Carpenter 2000): α, δ = $5^{\rm h}35^{\rm m}14\overset{\rm s}{.}57$,$-5^{\rm o}23'50\overset{''}{.}8$. Recently, an X-ray source (F421, Feigelson et al. (2002)) has been found to be coincident with this near IR source. However, there is still not definitive proof as to the particular driving source as neither of these sources lies directly in line with the flow of HH 529.

into the ionized zone.

The dynamical age of the HH 529 system can be calculated from the average proper motion (25 mas yr^{-1}). Assuming that the proper motion has remained constant over the 36″ from its point of origin, we find the dynamical age of the eastern-most visible feature of HH 529 to be roughly 1500 years. All shock model timescales will need to be consistent with this dynamical age in order for the model to be valid (§ 4).

As was recognized by O'Dell et al. (1997), the fact that this and other Orion nebula HH flows appear strongly in [O III] (atypical of most HH flows which show much lower ionization) suggests that these shocks are photoionized. We examine the physical conditions of HH 529 by comparing our high-resolution echelle spectra with (matter-bounded) photoionization models of this feature. Other studies of non-photoionized HH flows show evidence for a decrease in the amount of Fe depletion in some of the shocks, as determined from [Fe II] lines (Böhm & Matt 2001; Beck-Winchatz et al. 1996). This has been linked to grain destruction as matter originating from the molecular cloud passes through the shocks. In this paper, we assess the Fe depletion using a set of [Fe III] lines in the eastern-most feature of HH 529.

2. Observations

Spectra were obtained using the echelle spectrograph on the 4m Blanco telescope at CTIO (see Baldwin et al. (2000) for details) covering the spectral range from the near-UV (3500Å) to the near-IR (7500Å). Three sets of red and blue spectra were obtained on two dates in 1997 and 1998. One of the three slit positions (x2, see Fig. 1) intentionally overlaps with the eastern-most visible feature of HH 529. Wavelength and flux calibrations were performed as in Baldwin et al. (2000). We also used archival flux-calibrated (O'Dell & Doi (1999) using Baldwin et al. (1991)) HST WFPC2 associations (F487N, F502N, F547N, F631N, F656N, F658N, F673N) and Bally mosaics of these associations (less F487N). As there were a series of discrepant exposure times in the image headers of the Bally mosaics, the flux calibration had to be redone – again using the ground-based spectroscopic results of Baldwin et al. (1991) – to determine the relevant exposure times. With these exposure times in hand, all WFPC2 pixel brightnesses (from both Bally mosaics and archival WFPC2 associations) have been accurately converted to absolute fluxes/surface brightnesses, matching the ground-based flux calibration of Baldwin et al. (1991).

Looking at the spatially-resolved 'x2' echelle spectra, we have noticed two distinguishing features associated with the shock feature: a wide (5″) velocity-shifted component and a narrow (2.″5) velocity bridge seemingly connecting the nebula and the shock. Such a bridge

feature – which can also be seen in Fig. 6 of BOM – appears only to be associated with the leading optically visible shock. As this feature is intrinsically narrow (1.″5 from WFPC2 images), we have been able to determine the effective seeing for the red and blue spectra by measuring the width (along the slit) of the He I 5876 bridge feature – a line that is found in both the red and blue spectra (see Fig. 2). The seeing was slightly different on each of the two observing nights: 2″ for the red observations and 2.″5 for the blue. We can also see from this figure that the blue and red slits are aligned along their lengths to an accuracy of $\sim 0.''2$. However, there are small differences in the absolute observed flux, most probably as a result of a position difference in the transverse direction, along the shock feature. These deviations will be addressed in § 2.1.

A direct comparison of spatial variation in ground-based and space-based observations over the same wavelength range was made to confirm that the flux calibration of the echelle spectra is robust and that the slit alignment and orientation are correct. The echelle spectra were extracted over the same wavelength bandpass as the F656N WFPC2 filter. With knowledge of the approximate slit position (from a Polaroid of the slit against the nebular background), the F656N flux-calibrated image was used to re-create the expected spatial variation along the slit. This re-created profile was convolved with an appropriate-width (2″) Gaussian to simulate the seeing of the ground-based observations (see Fig. 3). This processing allows for direct comparison between ground- and space-based observations. (Note that there has been no continuum (or line contamination) subtraction from either the echelle spectrum or the WFPC2 reproduction, so the surface brightnesses in Fig. 3 are not those of Hα.) The slit's position on the F656N WFPC2 image was adjusted – while maintaining the slit orientation, $PA = 116^{\rm o}$ – so as to emulate more accurately the ground-based echelle slit spatial variation. This required only a slight adjustment ($< 1''$) of the slit from its original position on the WFPC2 image. Using the slit position determined from this analysis, we compared all WFPC2 filters with their respective portions of the ground-based spectra, resulting in accurate reproductions of both the spatial variation and absolute flux.

The high-resolution echelle spectra allow us to analyze the spatial variation of the nebula and shock separately – offering insight not possible from the WFPC2 photometry. For example, the slit variation of the [O III] 5007 and [O II] 3726 shock fluxes are shown in Fig. 4. Differences in variation across the slit between these two ions may be indicative of a higher density at the eastern-most edge of the shock: a higher density would lead to more recombinations and a slightly higher ionization fraction for O^+.

These WFPC2 and shock component analyses suggest that 10 pixels ($-0.''5$ to $+4.''0$) along the slit should be extracted in order to obtain the best contrast between the background nebular component and the velocity-shifted shock component (referred to hereafter as simply

the 'nebular' and 'shock' components). Following this extraction, and with the nebular line identifications from Baldwin et al. (2000) as a guide[2], the 'x2' spectral features were fit with two Gaussian components representing the nebular and shock components, as was done by Doi et al. (2004). Eight parameters were used in the fit: FWHM, peak wavelength and area for both components, and two parameters to fit the continuum baseline level and slope. The result of such a fit is shown in Fig. 5.

For cases where the shock component had a low signal-to-noise ($S/N < 5.2$), the lines were re-fit with a constrained double Gaussian. The strong nebular component of the constrained fit had no constraints while the weaker shock component's FWHM was fixed using the weighted average of the stronger lines' FWHM (28.3 km s^{-1}). The constrained velocity of the shock component was set using the weighted mean of the H I shock components (-42.1 km s^{-1}), and was maintained as a constant relative to the H I gas. Because of the ionization/velocity structure along the line-of-sight (Baldwin et al. 2000), the actual velocity differences between the weak shock component and the strong nebular component depend on the ion. If the S/N of the shock component improved and remained above 2.6, the constrained fit was used. Otherwise the double Gaussian fit was used for all lines with $S/N_{shock} > 2.6$.

If the double and constrained Gaussian fits resulted in an undetectable shock component ($S/N < 2.6$), a five-component (FWHM, peak wavelength, area, continuum baseline and slope) single Gaussian fit was used for the nebular line. The results of the line-fitting models are shown in Table 1 with nebular (neb) and shock (sh) components included in separate consecutive rows for each ID wavelength. Column descriptions are included in the table

The shock component can be seen most prominently in the medium-ionization forbidden lines (e.g., [O III]) as well as in the He I and H I permitted lines. Although the shock component can also be seen in the low-ionization lines ([O II], [N II]), its strength relative to the nebular line is much weaker (see Column (9) of Table 1). Of lines normally associated with the ionization front (IF) of photoionized gas, some [S II] can be seen very weakly in the shock component, whereas others ([N I]) are too weak to be detected. As will be discussed, the presence of [S II] does not imply an ionization front in the shock.

Unfortunately, the [O I] sky lines[3] lie close to the wavelength where the shock component would be. Using a triple Gaussian fit for the nebula, shock and sky components, we can

[2]All ID wavelengths are from Atomic Line List v2.04 (http://www.pa.uky.edu/~peter/atomic/, maintained by P. A. M. van Hoof), except [O II] (Blagrave & Martin 2004).

[3]These lines are identified as such from sky spectra and other nebular spectra (at positions which did not have a velocity-shifted feature) that were taken on the same evening.

determine if there is a detectable shock component for the [O I] 6300 line. The sky line FWHM, wavelength and area constraints are set by the sky line in the 1SW echelle spectrum taken on the same evening; the shock is constrained as in the constrained double Gaussian case. Following the fit of the three components in [O I] 6300, the shock component has a null detection ($S/N \ll 2.6$) lying well below our detection limit. Neither is there a detectable bridge component as seen with the other shock lines. It can be safely said that [O I] (as with [N I]) line emission in the shock lies below the detection limit for these spectra (*i.e.*, $S/N < 2.6$).

At first sight this seemed at odds with the BOM HH 529 [O I] observations depicted in their Figure 6 (WFPC2 631N image and Keck HIRES spectrum). However, their detection of [O I] with the 631N filter is not definitive due to contamination from the [S III] line (λ6312) (O'Dell & Doi 1999). BOM's original HIRES spectrum shows a strong [S III] velocity-shifted feature ($v \sim -39$ km s^{-1}) associated with the eastern-most shock of HH 529 (O'Dell, private communication, 2005). We also detect this in our spectrum and have determined quantitatively that [S III] would explain the presence of the shock in the WFPC2 631N image. Furthermore, the [O I] velocity contour plot displayed in BOM Fig. 6 is actually an inadvertent copy of the [O III] plot (O'Dell, private communication, 2005). The correct [O I] contours are similar to the [S II] contours in the west but have no velocity-shifted feature in the east.

2.1. Blue/red line strengths

Since the red and the blue spectra were taken on different nights, there is a slight pointing uncertainty (see Fig. 2) which makes comparison between the red and blue spectra more difficult. To study the uncertainties involved in inter-spectral comparison, we identified lines that are found in both the red and blue spectra. Six such lines had both a nebular and a measurable shock component ([Fe III] 5270, [Cl III] 5518, [Cl III] 5538, Si III 5740, [N II] 5755, and He I 5876). Table 2 summarizes the results from the (constrained) double Gaussian line-fitting for these seven lines prior to applying the reddening correction. The blue/red ratios for the nebular and shock components are each shown separately in Column (8) of Table 2, in the same rows as the blue results.

The nebular lines measured from the blue spectrum are not any stronger than the red on average ($B/R_{avg}^{weighted} \sim 1.02 \pm 0.04$). However, the average blue/red ratio ($B/R_{avg}^{weighted} \sim 0.85 \pm 0.04$) indicates otherwise for the shock. This difference in blue/red ratios is not unexpected, as there is no reason to expect a correlation between surface brightnesses in the nebula and shock. Using these results, we make an across-the-board adjustment to all

the red shock lines such that the shock line strengths match between the red and blue (0.85 adjustment) – allowing for a complete (blue/red) analysis of the shock. No such correction is made to the nebular feature, whose blue/red ratio is consistent with 1.0.

2.2. Reddening

It is expected that the reddening of both the nebular and shock components is the same, being dominated by foreground material. However, prior to making the correction discussed in § 2.1, the nebula and shock had drastically different Hα/Hβ Balmer decrements: 4.99±0.04 and 6.72 ± 0.32, respectively. After adjusting the line strengths so there is congruity between the red and blue lines (§ 2.1) in the red and blue spectra and accounting for that uncertainty, these values become 5.1±0.1 and 5.7±0.4 for the nebula and shock, respectively. This justifies the use of the blue/red correction in § 2.1 and the use of the same reddening correction for both nebula and shock: $E_{B-V} = 0.3655$ (Martin et al. 2006). The surface brightnesses are corrected for reddening as in Martin et al. (2006) and these dereddened values are included in Column (7) of Table 1.

3. Analysis

3.1. Velocity

Figure 6 plots all the velocities determined from the shock components of the Gaussian fits. They are quite consistent, as expected since unlike the expanding nebular gas, there should be no velocity gradient in the shocked gas. The shocked H I lines are shifted by -42.1 ± 1.2 km s^{-1} relative to the nebular H I lines (see Table 1 and Fig. 6), or -54.1 ± 1.2 km s^{-1} relative to the PDR in the molecular cloud, and hence, relative to the OOS embedded within the cloud. This agrees with the radial velocity measurements made by Doi et al. (2004) for the roughly coincident position 167-359 HH 529: -52 to -54 km s^{-1} relative to the PDR/OMC-1.

The [Fe III] 5270 shock component (with $S/N \sim 10$) appears to be discrepant in Fig. 6, with velocities of -32.9 ± 1.1 (blue) and -31.9 ± 1.1 km s^{-1} (red). This anomaly has an impact on the apparent nebular velocity gradient of [Fe III] lines (see Fig. 10 in Baldwin et al. (2000)) and is taken up in Appendix A.

3.2. Temperature and density

Temperatures (in K) and densities (in cm^{-3}) are calculated from emission line ratios using the NEBULAR routines included within the iraf STSDAS package. These are summarized in Table 3, with the respective transition probabilities and collision strengths used in the calculations.

The T_e([O III]) and T_e([N II]) diagnostic lines can be seen in both the nebula and the shock, while the [O I] temperature diagnostic lines can only be seen in the nebula. The nebula temperature from the blue [O III] lines is $T_e^{\rm neb}([{\rm O\ III}]) \sim 8536^{+35}_{-33}$, whereas for the red [N II] lines, the temperature is higher, $T_e^{\rm neb}([{\rm N\ II}]) \sim 10672^{+53}_{-52}$. Although these temperatures come from the blue and red spectra respectively and therefore represent two slightly different lines-of-sight, the temperature rise with depth in the nebula is what is generally seen for other lines-of-sight, and is largely the result of a hardening of the radiation field as photons close to the ionization limit are attenuated preferentially. To complete the nebular temperature analysis, we have found $T_e^{\rm neb}([{\rm O\ I}]) \sim 8005^{+580}_{-408}$.

In the shock, the lines are weaker (in the case of [N II], much weaker) and therefore the calculated temperatures have much larger uncertainties. The [O III] temperature is 8366^{+252}_{-214}, and that found from the [N II] temperature diagnostic lines is consistent (within 1σ): 8784^{+1184}_{-729}. Since the shock is matter-bounded (see § 3.3), O^{++} ([O III]) and N^{+} ([N II]) are not distinct zones and the attenuation seen in the nebula is not possible.

The electron density can be calculated from the diagnostic lines ([O II] 3726, 3729; [S II] 6716, 6731; [Cl III] 5517, 5537) which are seen in the nebula and weakly in the shock. In the nebula, these three sets of density diagnostic lines cover slightly different ionization zones along a particular line-of-sight, but in the shock – because of the lack of distinct ionization zones – the densities are expected to characterize the same zone. However, because of the disparity between red and blue slit positions, the calculated densities are also being defined along slightly different lines-of-sight.

For the nebula, we get $N_e^{\rm neb}$[O II] $\sim 1939^{+50}_{-50}$ ($N_e^{\rm neb}$[O II] ~ 2164 using entire slit) from the blue [O II] lines. The red [S II] lines yield a much higher density, $N_e^{\rm neb}([{\rm S\ II}]) \sim 5896^{+404}_{-366}$ ($N_e^{\rm neb}([{\rm S\ II}]) \sim 5638$ using entire slit), and the [Cl III] lines yield an even higher density, $N_e^{\rm neb}([{\rm Cl\ III}]) \sim 12074^{+1300}_{-1118}$.

It has been noted in Esteban et al. (2004) that the use of Zeippen (1982) transition probabilities and Pradhan (1976) collisions strengths drastically increases the calculated N_e([O II]). Upon further investigation, we find that a change in the transition probabilities alone will bring about the same result. Using these older atomic data, we almost double the measured density: $N_e^{\rm neb}([{\rm O\ II}]) \sim 3811$, bringing it more in line with the densities as

measured from other indicators. Another reason for questioning the atomic data comes from the [O II] temperature – which we overestimate slightly due to the shocked component impinging on the nebular component in the line pairs at 7320 and 7330. Using the density as calculated from [O II] 3726/3729 (2000 cm^{-3}), $T_e^{\rm neb}$([O II]) $\sim$ 20000 K. However, with the larger density (4000 cm^{-3}) and the old atomic data, $T_e^{\rm neb}$([O II]) $\sim$ 15000 K. An even larger density is required to reduce the temperature to 10000 K. Note that these densities from [O II] and [S II] are probably larger than in the more relevant [O III] zone, because of a falloff of density in the expanding gas. A similar result appears when we use older transition probability data for the N_e([Cl III]) calculation. The density is reduced to a more consistent value: $N_e^{\rm neb}$([Cl III]) $\sim 7247^{+575}_{-519}$. To round out our discussion of density, we have looked at the density dependence of [Fe III] (following Keenan et al. (2001)) and O II (following Peimbert & Peimbert (2005)) lines. The results are consistent with the densities we see in the rest of the nebula: $N_e^{\rm neb}$([Fe III]) $\sim 4700^{+800}_{-800}$ and $N_e^{\rm neb}$(O II) $\sim 6700^{+100}_{-100}$.

The density of the shock is also calculated, but as the low-ionization lines are weak, this calculated density is very uncertain. The blue [O II] lines yield $N_e^{\rm sh}$([O II]) $\sim 2898^{+8429}_{-1997}$, the red [S II] lines yield a density near the limits of this diagnostic ratio, $N_e^{\rm sh}$([S II]) $\sim 13183^{+10000}_{-11183}$, [Cl III] lines yield $N_e^{\rm sh}$([Cl III]) $\sim 21715^{+39170}_{-9641}$, and the [Fe III] lines yield[4] $N_e^{\rm sh}$([Fe III]) $\sim 7300^{+8000}_{-4100}$. (The O II lines are too weak to yield a consistent estimate of the shock density.) Use of the older atomic data again results in a higher [O II] density, $N_e^{\rm sh}$([O II]) $\sim$ 7304, and a lower [Cl III] density, $N_e^{\rm sh}$([Cl III]) $\sim$ 10911. The shock density appears to be larger (by roughly a factor of two) than that of the nebula, but given the large uncertainties, a density identical to that of the nebula is also allowed by the line ratios. Density will be revisited in a discussion of shock models in § 4.

3.3. Relative line strengths and ionization structure

To maximize the shock-to-nebula ratio, the echelle spectra were extracted over only half the slit. Even then, the echelle spectra maintain a weaker shock component as compared to the nebular component (see Column (9) of Table 1), indicative of a lower density, or more probably, a shorter emitting column in the shock. Since the illumination of the shock is roughly the same as that of the nebula, if the shock were optically thick, the shock-to-nebula ratio would be close to one for all lines, barring minor changes due to differences in density

[4]The lower limit is set using [Fe III] 4986 which is not observed in the shock. This indicates that I_{4986} is below the detection limit ($I_\lambda/I_{6678} \sim 0.01$, or $I_\lambda/I_{4658} \sim 0.05$), resulting in a minimum density of 3200 (Keenan et al. 2001).

(near the critical density) or changes due to abundance (see § 5). Here, the shock-to-nebula ratio is clearly lower than one, and so the shock is matter-bounded.

The relative strength varies from 0.2 for the medium-ionization lines (e.g., [O III]) to less than 0.03 for the low-ionization lines (e.g., [N II]) to below the detection limit for the lines usually associated with the ionization front (e.g., [N I]) and is plotted as a function of ionization potential in Fig. 7. In the case of a shortened emitting column, the ionization potential serves as an indicator of ionization fraction (where higher ionization potential indicates higher ionization fraction) while the shock-to-nebula ratio is a measure of the optical thickness of the shock to the relevant ionizing radiation. H I is presented as a standard for shock/nebula ionization comparison as its originating ion (H^+) has an ionization fraction of roughly one throughout both the shock and the nebula. The ratios of the medium-ionization species ([O III], [Ar III], [Ne III]) all lie above H I as they have a higher net ionization fraction in the shock than in the nebula column. However, none of these ratios is unity either. Thus, for example, in the shock there is not a complete O^{++} zone, preceding a distinct O^+ zone. The ratios of the low-ionization species ([O II], [N II], [S II]) lie below H I as they have a lower ionization fraction in the shock than in the nebula. In fact, they must arise from trace ionization stages in a more highly ionized zone (e.g., trace O^+ in the O^{++} zone). This is in contrast to the nebular column in which lines arise from distinct ionization zones. The lack of an ionization front tracer ([N I]) in the shock component provides further corroboration for a matter-bounded shock.

The critical densities associated with the [O II], [S II] and [Cl III] line transitions need to be considered as these lie within the expected density range of the shock and so collisional de-excitation could contribute to the relative weakness of the shock lines. However, the weak [N II] lines have critical densities of 7.8×10^4 and 1.2×10^7 cm^{-3} which lie well above the model-predicted density as discussed in § 4. The predominant cause of weakness is the lack of parent ions in this highly-ionized matter-bounded geometry.

3.4. Temperature fluctuations

Temperature fluctuations (t^2), first defined/introduced by Peimbert (1967), have been popular in explaining the differences in abundances found from forbidden lines as compared to those found from permitted lines. Although these fluctuations have been deduced to exist, their deduced size ($t^2 \sim 0.02$) has not been explained. Ferland (2001) has suggested a possible link with additional photoelectric heating from grains. Other suggestions – large scale variations in T_e, or the presence of regions either shielded from direct illumination by θ^1 Ori C or heated by shocks (from SNe mainly) – might explain temperature fluctuations

in the nebula, but not in a small-scale shock.

O II permitted and [O III] forbidden lines can be used to infer a value of t^2 as has been done by Esteban et al. (1998) and Esteban et al. (2004) for the nebula. We apply this to the shock too, adjusting our permitted line analysis to allow for deviations from LTE (Peimbert & Peimbert 2005). First, we must confirm that the nebular and shock O II permitted lines form following recombination (Grandi 1976). The shock-to-nebula ratios of the O II and [O III] lines are the same, and much larger than the shock-to-nebula ratios of the [O II] lines. Also, note that the velocities of the O II lines are consistent with the velocities of [O III] in the nebula (Table 1). These two observations both confirm that the O II lines are actually a result of recombinations from O^{++} and not a result of direct starlight excitation of O^{+}, validating the use of these lines in the determination of the O^{++}/H^{+} ratio. We have used O II recombination line multiplet 1 and [O III] collisionally-excited lines 4363, 4959 and 5007 with the NEBULAR[5] routines in IRAF (as in Esteban et al. (1998, 2004)) to determine t^2 for the nebula and the shock. Not all permitted lines of O II multiplet 1 are observed, so individual (or pairings of) recombination lines are used to predict the complete multiplet's relative surface brightness (see Table 4), following Peimbert & Peimbert (2005) (their equations 3 and 4). Using case A and case B O II recombination coefficients from Storey (1994) and case B H I recombination coefficients from Storey & Hummer (1995), O^{++}/H^{+} is calculated (see Table 4).

The O^{++}/H^{+} abundances from recombination and collisionally-excited lines and the inferred t^2 are summarized in Table 5 for both the nebula and the shock (along with the O^{+}/H^{+}, O^{0}/H^{+} and total O/H abundances). Our nebular t^2, 0.009 ± 0.004, is much lower than what has been deduced from another line-of-sight (for the same O^{++} ion), $t^2 \sim 0.020 \pm 0.002$ (Esteban et al. 2004) – which did not correct O II lines for deviations from LTE. Despite the presence of detectable O II lines in the shock, the uncertainties are large enough that there is only a 1σ "detection" of t^2 in the shock, $t^2 = 0.010 \pm 0.010$. If the grains are depleted in the shock, a detectable t^2 suggests that the grains may not be the main contributor to t^2. This will be followed up in § 5.2.

[5]The collisionally-excited line results were calculated using the three-zone model in IRAF. In this case only the low- and medium-ionization zones (those of $O^{0}/O+$ and O^{++}) are of interest. The adopted densities of the nebula and shock are $N_e = 6000$ and 10000, respectively. The temperatures are those determined from the [N II] and [O III] temperature diagnostic lines (refer to § 3.2) for the low- and medium-ionization zones, respectively.

4. Models

The HH object has been shown to be photoionized, so we can model the emission using the radiative-collisional equilibrium code, Cloudy. As the [Fe III] lines figure prominently in our discussion, we have improved the description of the Fe^{++} atom in Cloudy from a two-level to a 14-level atom, using collision strengths and transition probabilities from Zhang (1996) and Quinet et al. (1996) respectively. This allows all multiplet lines associated with λ4658 and λ5270 to be included in the determination of Fe abundance. Also, as the accuracy of the atomic data for O^+ has been questioned (§ 3.2, Esteban et al. (2004)) we have replaced the up-to-date transition probabilities (Wiese et al. 1996) with the older ones (Zeippen 1982).

Baldwin et al. (2000) showed that the incident continuum radiation (from the ionizing star, θ^1 Ori C) is best represented by a Mihalas stellar atmosphere model. However, to test the robustness of our result, we also developed models using a Kurucz stellar atmosphere. Note that the issues with the Kurucz atmosphere (primarily with its inability to accurately predict the high ionization line [Ne III] 3869) are not that relevant to our discussion of low- and medium-ionization species.

Since the shock has a small covering factor compared to the nebula, spherical geometry is not assumed and an inner radius is not set. The sound-crossing time for the HH feature ($\sim 10^3$ years) is roughly the same order as the dynamical timescale of the flow (1500 years), so instead of assuming a constant pressure (as would be the case in a nebular model), we assume a constant density. Also, as the flow has only been in existence for 1500 years (5×10^{10} s), it is important to check the validity of a photoionization equilibrium code. The longest timescale from the Cloudy shock model comes from H-recombination: 2×10^8s – well within the limit of the flow's age. The incident surface flux of ionizing photons, $\phi(H)$ should be close to the value derived for nebular models ($\log\phi(H) \sim 13.0$, *e.g.* Baldwin et al. (1991)) as the shock is roughly the same distance from θ^1 Ori C as the nebula (see § 1). However, the electron density is probably significantly higher in the shock than in the nebula as evident from the observed λ6731/λ6716 ratios. Since the shock has been shown to be matter-bounded and homogeneous with respect to its ionization structure (§ 3.3), the shock model can be developed simply as a finite thickness truncated nebula (i.e., with a pre-defined stopping thickness). This thickness can be predicted from the length ($10''$) and width ($2''$) of the shock in the plane of the sky (from [O III] WFPC2 image) and its assumed cylindrically-symmetric geometry. Adopting a distance to the nebula of 460 pc (BOM), the predicted median depth ($3''$) translates to a thickness of 0.007 pc (2×10^{16} cm).

The parameters are varied from these initial values, using observed surface brightness of He I 6678, and line ratios indicating temperature, density and ionization (see Table 6) to determine the best-fit models. In the case of an optically thin model, the surface brightness

varies as $n_H^2 t$, where n_H is the hydrogen density and t is the model thickness. Adjusting the model thickness does not result in (much of) a change to any of the other constraint ratios as the ionization fractions of most species are constant through the entire model. Therefore, t is not completely independent, leaving $T_\star$, $\phi(H)$ and n_H as the three independent parameters.

A series of models were developed, two of which are summarized in Table 7: one with a Mihalas stellar atmosphere and Cloudy Orion abundances (from Baldwin et al. (1991); Rubin et al. (1991); Osterbrock et al. (1992)); and one with a Kurucz stellar atmosphere and Esteban et al. (2004) Orion abundances (see Table 8). After determining the best-fit parameters for both of these models, the Fe abundance was adjusted to fit the series of [Fe III] lines using the Cloudy *optimize* routine. Some implications of the derived abundances will be discussed in § 5.1.

5. Discussion

The echelle observations (from Table 1) and the model predictions are summarized in Table 9 as I_λ/I_{6678}. If there is no model prediction (i.e., the particulars of the line formation are not included in the model) then the observations are not included in the table.

It is informative to compare the model predictions with the echelle observations for not only the constraint ratios, but all lines predicted by the model. This will further test the robustness of the model. Special note should be taken of lines predicted to be seen in the shock, but not observed. Of such cases, many of them appear around or below the detection limit ($I_\lambda/I_{6678} \sim 0.01$). Many of those lines predicted to be above this limit (He I 3705, [S III] 3722, H I 3722, He I 3889, He I 4009, [S II] 4076, C II 4267, O II 4341, [O II] 7320, [O II] 7331) appear as blended line features in the spectrum and therefore are not included in Table 9. There are another three undetected-but-predicted shock lines: O II 4093, O II 4111, O II 4277. Each of these is a complete multiplet prediction requiring a series of multiplet correction factors to predict the observed multiplet component lines. After applying these correction factors to the shock model lines, their predicted flux would lie below the observed detection limit. As discussed in § 2, the velocity-shifted [O I] lines are sky lines and not associated with the shock, explaining the disagreement between observation and model at [O I] 6300.

5.1. Depletion

The Orion nebula is thought to have a depleted gas-phase abundance of Fe of roughly a factor of 10 (with respect to solar) due to the presence of grains. From a preliminary analysis, this does not appear to be the case for the shock. The ionization fraction of Fe^{++} remains roughly constant through the slab ($Fe^{++} \sim 0.2$, Figure 8) with no well-defined Fe^{++} zone, and yet the [Fe III] lines appear quite strong relative to the nebula lines (see Figure 7). This may indicate an "undepletion" of Fe (possibly up to the solar level).

A series of [Fe III] lines (λ4658, λ5270, etc.) is predicted using the higher resolution Fe^{++} ion (§ 4) and numerous [Fe II] lines are predicted using the 371-level Fe^{+} ion. These [Fe II] lines have been shown to have large contributions from continuum pumping Verner et al. (2000) and therefore, cannot be used as indicators of Fe abundance, but the modelled [Fe III] lines scale linearly with the Fe abundance. The iron abundances determined from matching the observed and modelled [Fe III] lines in both shock models appear to be roughly consistent with the nebular gas-phase Fe abundance (see Table 10) indicating that the seemingly high shock [Fe III] line strengths can mostly be explained by differences in the models' parameters, not needing to resort to an order of magnitude change in the abundance. However, if the nebular Fe/H gas-phase abundance is as low as 6.23 (Esteban et al. 2004), the extreme prediction of Model B would suggest a three-fold increase in Fe/H gas-phase abundance indicating a partial destruction of grains in the shock.

An analysis of the Fe abundance of Orion B stars (Cunha & Lambert 1994) and a follow-up analysis of Orion F and G stars (Cunha et al. 1998) imply that the total abundance of Fe is consistent from star to star within the Orion association, but that there may be a slight total Fe depletion with respect to solar (-0.16 dex, Cunha et al. (1998)). The Fe depletions obtained from our shock analyses are greater, ranging from -0.8 to -1.0 dex with respect to solar – on the order of the depletions found in the nebula (Baldwin et al. 1991; Rubin et al. 1997; Esteban et al. 1998, 2004). Assuming that the total Orion Fe abundance is on the order of that found from the Orion association stars, the majority of the iron in the shock, as in the nebula, must be locked up in grains.

A number of Si lines are also seen in the shock. Although there is no Cloudy prediction for these Si lines, the observations can still be analyzed using ionization models from Cloudy and line information from Grandi (1976). The shock-to-nebula ratio is high ($\sim$ 0.15) for Si II 3856, 5056, 6347 (and 6371), but these lines have been shown to form due to starlight excitation (Grandi 1976) in the Si^{+} gas. The Si^{+} ionization fraction predicted from the Cloudy models (0.03) is much less than that for Fe^{++} (0.2), but the Si II lines are not linearly dependent on Si abundance so these lines alone can not be used to determine Si abundance.

Since $\sim$ 20% of O atoms are thought to be in dust grains (Esteban et al. 2004), the gas-phase abundance of O can be analyzed to determine the extent of dust destruction. The total O/H in the nebula and in the shock is summarized in Table 5. Note that O/H for the shock component (8.73 ± 0.05) is an upper limit and the actual value is most likely closer to that of O^{++}/H^{+} (8.69 ± 0.05). The shock [O II] and [O III] line profiles across the extracted part of the slit peak at different spatial positions (see Fig. 4), indicating that these lines are tracing physically different lines of sight and that a simple addition of O^{++} and O^{+} may overestimate the O/H abundance. Our observed nebula O/H abundance (8.48 ± 0.01 or 8.52 ± 0.03 using recombination lines) deviates slightly from other Orion nebula observations, which find O/H$\sim 8.60 - 8.65$ (Baldwin et al. 1991; Rubin et al. 1991; Osterbrock et al. 1992; Esteban et al. 2004). The shock O/H abundance should be compared to an average/typical O/H nebula abundance, as the shock originates in a different region of the nebula. For our observations of the shock, the uncertainty in O/H is large enough that no definitive statement can be made with regards to dust destruction in the shock, except that there may be a small "undepletion" of gas-phase O to parallel the "undepletion" of gas-phase Fe.

Smith et al. (2005) have imaged the bow shocks of HH 529 with T-ReCS at 11.7μ, seeing what they refer to as "most likely thermal dust emission" associated with the eastern-most shock. Although supporting the argument of Smith et al. (2005), our evidence for the existence of grains in this one HH object is anomalous when compared with the 21 HH objects studied by Böhm & Matt (2001). For both their high-excitation/fast-moving ($v > 85$ km s^{-1}) and low-excitation/slow-moving ($v \leq 50$ km s^{-1}) HH objects, the derived Fe depletion is never more than -0.4 dex suggesting that the grains are most likely destroyed in the HH objects regardless of their velocity. It is of interest that for HH 529 – measured to have a velocity of 76 km s^{-1} relative to OMC-1 – the depletion is on the order of that of the nebula (-1.0 dex); there is no evidence for the complete destruction of grains in the eastern-most visible shock of HH 529. This is more along the lines of what one would expect: a slow-moving flow would not be expected to destroy grains, whereas a fast-moving flow would. Böhm & Matt (2001) suggest that the molecular cloud material currently associated with their slow-moving shock may have had its grains destroyed in an earlier pass through a faster-moving shock. Following this argument, the material associated with HH 529 must not have ever passed through a high-excitation/fast-moving shock. This is slightly inconsistent with the set of HH 529 velocities measured by Doi et al. (2002, 2004), many of which suggest the material may have been travelling faster than 85 km s^{-1}. A full Fe abundance analysis of all HH 529 shocks could offer further insight into grain destruction in Herbig Haro objects.

5.2. Temperature fluctuations

The t^2 deduced to exist in the nebula is 0.009 ± 0.004 and in the shock is 0.010 ± 0.010 (§ 3.4) (which are both within 2σ of zero). Two suggested explanations for the existence of t^2 – large scale variations in T_e or the presence of shielded or heated regions – can not apply for the small column covered by the shock. However, since the grains still appear to be present in the shock a t^2 detection suggests a third explanation: that the grains may be the main contributor to t^2. Conversely, an "effective" t^2 may be introduced if the effective recombination coefficients, collision strengths and/or transition probabilities are inaccurate, or if there were some other contributions to the line emission besides solely recombination or collisional excitation.

6. Conclusions

High-resolution spectroscopy of the Orion nebula across the Herbig Haro object HH 529 has allowed for a comparison of that local part of the nebula with the velocity-shifted spectrum of the flow. The radial velocity (as measured from the H I emission lines), -42.1 ± 1.2 km s^{-1} is consistent with the -40 to -42 km s^{-1} range as measured by Doi et al. (2004) for a slightly different line-of-sight. In addition, there is ample evidence to suggest that this flow has been photoionized. Herbig Haro objects usually have a strong low-ionization line spectrum. In this case, the fact that we see strong medium-ionization lines and much weaker low-ionization lines indicates that we have a photoionized shock, as first suggested by O'Dell et al. (1997). The distinguishing shock-to-nebula ratios as a function of ionization fraction, or ionizing potential as in Figure 7, further support this hypothesis, leading us to model the shock as a matter-bounded photoionization region.

The shock component was modelled using the photoionization equilibrium code, Cloudy. Both Mihalas and Kurucz stellar atmosphere models were investigated to ensure the robustness of our conclusions. A series of "best-fit" models covering a range of stellar temperatures, densities, and $\phi(H)$ fluxes has allowed us to determine that the depletion of Fe (relative to solar) in the nebula also exists in the shock. The higher density of the photoionized shock allows for the formation of relatively strong [Fe III] lines without necessitating a reduction of the Fe depletion. The Fe depletion for the shock is roughly the same as for the Orion nebula, an order of magnitude relative to solar (-1.0 dex). The total Fe abundance of the Orion association stars may be slightly depleted (-0.16 dex, Cunha et al. (1998)), but not to the extent of the gas-phase Fe in the nebula and shock. This suggests that if the total Fe abundance in the nebula and shock is of the same order as that found from the Orion association stars, grains must be present in the Herbig Haro flow to account for the depletion

of gas-phase Fe. Böhm & Matt (2001) suggests that grains are destroyed in many HH objects as the material passes through high-excitation/fast-moving shocks. From our results, we infer that the eastern-most shock of HH 529 never reached the velocities necessary to destroy the majority of the grains despite the presence of fast-moving shocks elsewhere in HH 529. This supports the observations of 11.7μ thermal dust emission in the eastern-most shock of HH 529 (Smith et al. 2005). Further information about grain destruction in HH 529 can be obtained from parallel Fe abundance analyses for the remainder of the HH 529 photoionized shocks.

Temperature fluctuations in the Orion nebula have been used to explain discrepancies in abundances found from recombination lines versus abundances found from collisionally-excited lines. Using solely lines originating from the O^{++} gas, we derive t^2 for the nebula ($t^2 = 0.009 \pm 0.004$) and the shock ($t^2 = 0.010 \pm 0.010$). Esteban et al. (2004) have published a series of t^2 for a number of ions, including O^{++} (0.020 ± 0.002), as well as an average from their series of ions (0.022 ± 0.002). The interesting result is that the shock maintains a t^2 similar to the nebula (albeit with a large uncertainty) despite being much thinner. These observations, if corroborated with higher S/N data, may draw into question some of the theories that have been expounded surrounding an explanation for these inferred t^2 fluctuations. Grains appear to be present in the shock, suggesting that the grains may still somehow be contributing to t^2. The measurement of a non-zero t^2 in a matter-bounded shock would more likely support the argument for an "effective" t^2 resulting from uncertainties in the atomic data and/or missing contributions to the line emission. Higher S/N O II spectra of the shock will reduce the uncertainty of the inferred t^2, and allow for more definitive conclusions to be made.

This work was supported by the Natural Sciences and Engineering Research Council of Canada. Line wavelengths were obtained from the Atomic Line List[6] maintained by P. A. M. van Hoof. Calculations were performed with version 05.07 of Cloudy, last described by Ferland et al. (1998). The authors wish to thank C. R. O'Dell for his clarification of a portion of the BOM data, and referee M. Peimbert for his detailed review of this paper.

A. Revisiting [Fe III] energy levels

As there is no velocity gradient in the shock, all shock lines should have the same velocity relative to the H I lines in the nebula. However, a velocity discrepancy associated with the

[6]Atomic Line List v2.04 is available at: http://www.pa.uky.edu/~peter/atomic/.

[Fe III] 5270 line appears in Figure 6. The most obvious explanation for this is that the ID wavelength for the [Fe III] 5270 is wrong because of an error in the adopted energy of the upper $^3P_2^4$ energy level. The other line originating from the same upper level, [Fe III] 5412 is much weaker and therefore the velocity of the shock component cannot be measured as reliably. However, a constrained Gaussian with a shock velocity that is consistent with that observed in [Fe III] 5270 does appear to fit the data well, albeit with a $S/N \sim 3$ for the shock component. The $^3P_2^4$ energy is quoted as 19404.8 ± 0.5 cm^{-1} (Sugar & Corliss 1985). This uncertainty translates to ± 0.14Å, or ± 7.9 km s^{-1} for both [Fe III] 5270.40 and [Fe III] 5411.98. The red and blue observations were used to constrain the energy of this common upper level, fixing the energies of the lower levels at their NIST values[7]. For these lines to have a velocity consistent with that of the shock (-42.1 km s^{-1}), $^3P_2^4$ must be 19404.44 ± 0.26 cm^{-1}.

This is interesting in the context of the Fe^{++} velocity gradient presented in Baldwin et al. (2000). A velocity gradient of [Fe III] initially observed as a function of wavelength was re-interpreted to be a velocity gradient as a function of the lines' upper level excitation potential above the ground state. The interpretation was presented with scepticism as there was no evidence (or explanation) for velocity gradients associated with any other single ion. The adjustment of the $^3P_2^4$ term lowers the nebular velocity of [Fe III] 5270 and [Fe III] 5412 to that of the other [Fe III] lines (~ 4 km s^{-1}), removing most of the evidence for a velocity gradient. Note that this nebular velocity is consistent with what is expected from the relationship between velocity and ionization potential (Baldwin et al. 2000).

The only remaining evidence for a sharp velocity gradient in the Fe^{++} zone is from the lines with $^3G_4$ (24940.9 cm^{-1}, (Sugar & Corliss 1985)) as their common upper level ([Fe III] 4008, [Fe III] 4080). The same uncertainty (± 0.5 cm^{-1}) exists for this level, translating to uncertainties in the ID wavelengths of [Fe III] 4008.35 ± 0.08 and [Fe III] 4079.70 ± 0.08, or equivalently to an uncertainty in the velocity: ± 6.1 km s^{-1}. These two lines are too weak to be measured in the shock, but for their line velocities to be consistent with the nebula [Fe III] velocities, $^3G_4$ would have to be 24941.37 ± 0.23, $\sim 1\sigma$ above the accepted mean (Sugar & Corliss 1985).

In summary, if we require the concordance of [Fe III] line velocities in the shock and in the nebula, the $^3P_2^4$ energy would be 19404.44 ± 0.26 cm^{-1} producing lines with air wavelengths 5270.50 ± 0.07 and 5412.08 ± 0.07. The $^3G_4$ energy would be 24941.37 ± 0.23 producing lines with wavelengths 4008.27 ± 0.04 and 4079.62 ± 0.04.

[7]http://physics.nist.gov/PhysRefData/ASD/index.html

REFERENCES

Böhm, K. & Matt, S. 2001, PASP, 113, 158

Baldwin, J. A., Ferland, G. J., Martin, P. G., Corbin, M. R., Cota, S. A., Peterson, B. M., & Slettebak, A. 1991, ApJ, 374, 580

Baldwin, J. A., Verner, E. M., Verner, D. A., Ferland, G. J., Martin, P. G., Korista, K. T., & Rubin, R. H. 2000, ApJS, 129, 229

Bally, J., O'Dell, C. R., & McCaughrean, M. J. 2000, AJ, 119, 2919

Beck-Winchatz, B., Böhm, K., & Noriega-Crespo, A. 1996, AJ, 111, 346

Bhatia, A. K. & Kastner, S. O. 1995, ApJS, 96, 325

Blagrave, K. P. M. & Martin, P. G. 2004, ApJ, 610, 813

Cunha, K. & Lambert, D. L. 1994, ApJ, 426, 170

Cunha, K., Smith, V. V., & Lambert, D. L. 1998, ApJ, 493, 195

Doi, T., O'Dell, C. R., & Hartigan, P. 2002, AJ, 124, 445

—. 2004, AJ, 127, 3456

Esteban, C., Peimbert, M., García-Rojas, J., Ruiz, M. T., Peimbert, A., & Rodríguez, M. 2004, MNRAS, 355, 229

Esteban, C., Peimbert, M., Torres-Peimbert, S., & Escalante, V. 1998, MNRAS, 295, 401

Feigelson, E. D., Broos, P., Gaffney, J. A., Garmire, G., Hillenbrand, L. A., Pravdo, S. H., Townsley, L., & Tsuboi, Y. 2002, ApJ, 574, 258

Ferland, G. J. 2001, PASP, 113, 41

Ferland, G. J., Korista, K. T., Verner, D. A., Ferguson, J. W., Kingdon, J. B., & Verner, E. M. 1998, PASP, 110, 761

Goudis, C. 1982, The Orion complex: A case study of interstellar matter (Dordrecht, Netherlands, D. Reidel Publishing Co. (Astrophysics and Space Science Library. Volume 90), 1982. 323 p.)

Grandi, S. A. 1976, ApJ, 206, 658

Grevesse, N. & Sauval, A. J. 1999, A&A, 347, 348

Hillenbrand, L. A. & Carpenter, J. M. 2000, ApJ, 540, 236

Kaufman, V. & Sugar, J. 1986, Journal of Physical and Chemical Reference Data, 15, 321

Keenan, F. P., Aller, L. H., Ryans, R. S. I., & Hyung, S. 2001, Proceedings of the National Academy of Science, 98, 9476

Keenan, F. P., Hibbert, A., Ojha, P. C., & Conlon, E. S. 1993, Phys. Scr, 48, 129

Lennon, D. J. & Burke, V. M. 1994, A&AS, 103, 273

Martin, P. G., Blagrave, K. P. M., Rubin, R. H., Ferland, G. J., Dufour, R. J., O'Dell, C. R., Baldwin, J. A., Hester, J. J., & Walter, D. K. 2006, in preparation

McLaughlin, B. M. & Bell, K. L. 1993, ApJ, 408, 753

Mendoza, C. & Zeippen, C. J. 1982, MNRAS, 198, 127

O'Dell, C. R. 2001a, PASP, 113, 29

—. 2001b, ARA&A, 39, 99

O'Dell, C. R. & Doi, T. 1999, PASP, 111, 1316

—. 2003, AJ, 125, 277

O'Dell, C. R., Hartigan, P., Bally, J., & Morse, J. A. 1997, AJ, 114, 2016

O'Dell, C. R. & Wong, K. 1996, AJ, 111, 846

Osterbrock, D. E., Tran, H. D., & Veilleux, S. 1992, ApJ, 389, 305

Peimbert, A. & Peimbert, M. 2005, in Revista Mexicana de Astronomia y Astrofisica Conference Series, 9–14

Peimbert, M. 1967, ApJ, 150, 825

Pradhan, A. K. 1976, MNRAS, 177, 31

Quinet, P., Le Dourneuf, M., & Zeippen, C. J. 1996, A&AS, 120, 361

Ramsbottom, C. A., Bell, K. L., & Keenan, F. P. 1999, MNRAS, 307, 669

Ramsbottom, C. A., Bell, K. L., & Stafford, R. P. 1996, Atomic Data and Nuclear Data Tables, 63, 57

Reipurth, B. & Bally, J. 2001, ARA&A, 39, 403

Rubin, R. H., Dufour, R. J., Ferland, G. J., Martin, P. G., O'Dell, C. R., Baldwin, J. A., Hester, J. J., Walter, D. K., & Wen, Z. 1997, ApJ, 474, L131

Rubin, R. H., Simpson, J. P., Haas, M. R., & Erickson, E. F. 1991, ApJ, 374, 564

Smith, N., Bally, J., Shuping, R. Y., Morris, M., & Hayward, T. L. 2004, ApJ, 610, L117

Smith, N., Bally, J., Shuping, R. Y., Morris, M., & Kassis, M. 2005, AJ, 130, 1763

Storey, P. J. 1994, A&A, 282, 999

Storey, P. J. & Hummer, D. G. 1995, MNRAS, 272, 41

Sugar, J. & Corliss, C. 1985, Atomic energy levels of the iron-period elements: Potassium through Nickel (Washington: American Chemical Society, 1985)

Verner, E. M., Verner, D. A., Baldwin, J. A., Ferland, G. J., & Martin, P. G. 2000, ApJ, 543, 831

Wen, Z. & O'Dell, C. R. 1995, ApJ, 438, 784

Wiese, W. L., Fuhr, J. R., & Deters, T. M. 1996, Atomic transition probabilities of carbon, nitrogen, and oxygen : a critical data compilation (Atomic transition probabilities of carbon, nitrogen, and oxygen : a critical data compilation. Edited by W.L. Wiese, J.R. Fuhr, and T.M. Deters. Washington, DC : American Chemical Society ... for the National Institute of Standards and Technology (NIST) c1996. QC 453 .W53 1996.)

Zapata, L. A., Rodríguez, L. F., Kurtz, S. E., O'Dell, C. R., & Ho, P. T. P. 2004, ApJ, 610, L121

Zeippen, C. J. 1982, MNRAS, 198, 111

Zhang, H. 1996, A&AS, 119, 523

Table 1. Summary of double Gaussian fits to observed echelle spectra.

ID Wave[a,b] (1)	ID (2)	?[c] (3)	Wavel[d] (4)	Velocity[e] (5)	FWHM[e,f] (6)	I_{corr}[g,h] (7)	S/N[i] (8)	I_{sh}/I_{neb}[j] (9)	Notes[k] (10)
3512.505	He I	?	3512.526	1.8 ± 1.7	19.1 ± 4.4	0.0718 ± 0.0167	4.3	0.6992 ± 0.2724	C
		?	3512.023	-41.1 ± 1.7	28.3 ± 0.0	0.0502 ± 0.0157	3.2		
...		?	3530.556	...	33.0 ± 9.9	0.1582 ± 0.0546	2.9	...	S
			...	...	...	...	...		
3554.389	He I		3554.424	3.0 ± 0.8	13.9 ± 1.8	0.1042 ± 0.0129	8.1	...	S
			...	...	...	...	...		
3587.253	He I		3587.281	2.3 ± 1.6	23.9 ± 4.1	0.2617 ± 0.0467	5.6	0.5319 ± 0.1723	C
		?	3586.767	-40.6 ± 1.6	28.3 ± 0.0	0.1392 ± 0.0376	3.7		
...		?	3599.206	...	31.3 ± 10.1	0.0523 ± 0.0174	3.0	0.9484 ± 0.3826	C
		?	3598.700	...	28.3 ± 0.0	0.0496 ± 0.0113	4.4		
3613.642	He I		3613.636	-0.5 ± 0.3	16.9 ± 0.9	0.2252 ± 0.0115	19.6	0.2091 ± 0.0561	C
		?	3613.135	-42.1 ± 0.3	28.3 ± 0.0	0.0471 ± 0.0124	3.8		
3634.241	He I		3634.231	-0.8 ± 0.5	19.4 ± 1.3	0.2391 ± 0.0158	15.1	0.1765 ± 0.0664	C
		?	3633.729	-42.2 ± 0.5	28.3 ± 0.0	0.0422 ± 0.0156	2.7		
3655.593	H I	?	3655.611	1.5 ± 1.8	25.5 ± 6.2	0.1160 ± 0.0446	2.6	...	S
			...	...	...	...	...		
3656.106	H I	?	3656.175	5.7 ± 1.3	13.6 ± 3.7	0.0409 ± 0.0124	3.3	...	S
			...	...	...	...	...		
3656.663	H I		3656.662	-0.1 ± 0.8	23.7 ± 2.4	0.0775 ± 0.0099	7.8	...	S
			...	...	...	...	...		
3657.267	H I	?	3657.302	2.9 ± 1.6	22.9 ± 4.7	0.0917 ± 0.0224	4.1	...	S
			...	...	...	...	...		
3657.923	H I	?	3657.920	-0.3 ± 2.4	22.6 ± 6.7	0.0809 ± 0.0289	2.8	...	S
			...	...	...	...	...		
3658.639	H I		3658.648	0.7 ± 1.6	28.9 ± 4.5	0.1088 ± 0.0205	5.3	...	S
			...	...	...	...	...		
3659.421	H I		3659.423	0.2 ± 1.1	19.6 ± 3.0	0.0752 ± 0.0121	6.2	...	S
			...	...	...	...	...		
3660.277	H I		3660.267	-0.8 ± 1.6	26.7 ± 4.2	0.1014 ± 0.0188	5.4	...	S
			...	...	...	...	...		
3661.218	H I		3661.237	1.5 ± 0.7	21.0 ± 2.0	0.1151 ± 0.0111	10.4	...	S
			...	...	...	...	...		
3662.256	H I		3662.235	-1.8 ± 1.0	27.7 ± 2.6	0.1287 ± 0.0130	9.9	...	S
			...	...	...	...	...		
3663.404	H I		3663.390	-1.1 ± 0.8	26.5 ± 2.2	0.1624 ± 0.0146	11.1	...	S
			...	...	...	...	...		
3664.676	H I		3664.677	0.1 ± 0.6	27.9 ± 1.5	0.1975 ± 0.0110	17.9	...	S
			...	...	...	...	...		
3666.095	H I		3666.085	-0.8 ± 0.5	24.9 ± 1.1	0.2409 ± 0.0117	20.6	0.1669 ± 0.0425	C
		?	3665.583	-41.9 ± 0.5	28.3 ± 0.0	0.0402 ± 0.0100	4.0		
3667.681	H I		3667.681	0.0 ± 0.6	30.2 ± 1.4	0.2748 ± 0.0139	19.8	0.1885 ± 0.0344	C
			3667.161	-42.5 ± 0.6	28.3 ± 0.0	0.0518 ± 0.0091	5.7		
3669.464	H I		3669.454	-0.8 ± 0.4	24.4 ± 1.0	0.2962 ± 0.0125	23.7	0.1286 ± 0.0352	C
		?	3668.949	-42.1 ± 0.4	28.3 ± 0.0	0.0381 ± 0.0103	3.7		
3671.475	H I		3671.472	-0.3 ± 0.4	27.1 ± 1.0	0.3229 ± 0.0118	27.4	0.1796 ± 0.0339	
			3670.958	-42.3 ± 2.0	25.2 ± 5.0	0.0580 ± 0.0107	5.4		
3673.758	H I		3673.755	-0.2 ± 0.3	26.2 ± 0.8	0.3341 ± 0.0111	30.0	0.1140 ± 0.0256	C
		?	3673.242	-42.1 ± 0.3	28.3 ± 0.0	0.0381 ± 0.0085	4.5		
3676.362	H I		3676.359	-0.2 ± 0.3	27.1 ± 0.9	0.3908 ± 0.0129	30.3	0.1592 ± 0.0254	C
			3675.845	-42.2 ± 0.3	28.3 ± 0.0	0.0622 ± 0.0097	6.4		
3679.352	H I		3679.345	-0.6 ± 0.2	28.7 ± 0.6	0.4524 ± 0.0094	48.2	0.1645 ± 0.0192	
			3678.808	-44.3 ± 1.1	25.2 ± 3.0	0.0744 ± 0.0086	8.7		
3682.808	H I		3682.797	-0.9 ± 0.2	25.3 ± 0.7	0.4455 ± 0.0124	35.8	0.1320 ± 0.0219	C
			3682.292	-42.0 ± 0.2	28.3 ± 0.0	0.0588 ± 0.0096	6.1		
3686.830	H I		3686.825	-0.4 ± 0.2	27.1 ± 0.7	0.5463 ± 0.0144	37.9	0.1353 ± 0.0205	C
			3686.310	-42.3 ± 0.2	28.3 ± 0.0	0.0739 ± 0.0110	6.7		
3691.554	H I		3691.544	-0.8 ± 0.2	26.2 ± 0.6	0.6167 ± 0.0128	48.3	0.1795 ± 0.0233	
			3690.964	-47.9 ± 1.4	27.8 ± 3.5	0.1107 ± 0.0142	7.8		
3694.212	Ne II	?	3694.151	-4.9 ± 1.0	5.1 ± 1.5	0.0173 ± 0.0060	2.9	...	S small FWHM
			...	...	...	...	...		
3697.152	H I		3697.156	0.3 ± 0.6	28.6 ± 1.4	0.6467 ± 0.0337	19.2	0.2013 ± 0.0381	C
			3696.637	-41.8 ± 0.6	28.3 ± 0.0	0.1302 ± 0.0237	5.5		
3703.852	H I		3703.850	-0.1 ± 0.2	25.6 ± 0.7	0.6863 ± 0.0198	34.7	0.1652 ± 0.0231	C
			3703.345	-41.0 ± 0.2	28.3 ± 0.0	0.1134 ± 0.0155	7.3		
3705.006	He I		3705.000	-0.5 ± 0.3	18.6 ± 0.7	0.3635 ± 0.0153	23.8	...	S avg
			...	...	...	...	...		

Table 1—Continued

ID Wave[a,b] (1)	ID (2)	?[c] (3)	Wavel[d] (4)	Velocity[e] (5)	FWHM[e,f] (6)	I_{corr}[g,h] (7)	S/N[i] (8)	I_{sh}/I_{neb}[j] (9)	Notes[k] (10)
3711.971	H I		3711.960	-0.9 ± 0.6	26.3 ± 1.4	1.0106 ± 0.0558	18.1	0.1941 ± 0.0435	C
		?	3711.437	-43.2 ± 0.6	28.3 ± 0.0	0.1962 ± 0.0427	4.6		
3713.080	Ne II	?	3713.057	-1.8 ± 0.7	7.6 ± 1.7	0.0206 ± 0.0044	4.7	···	S small FWHM
			···	···	···	···	···		
3721.938	H I		3721.824	-9.1 ± 0.7	38.4 ± 2.0	1.5474 ± 0.0949	16.3	···	S , [S III] line blend
			···	···	···	···	···		
3726.032	[O II]		3726.087	4.4 ± 0.1	18.8 ± 0.2	27.4591 ± 0.2373	115.7	0.0455 ± 0.0087	C
		?	3725.511	-41.9 ± 0.1	28.3 ± 0.0	1.2481 ± 0.2400	5.2		
3728.784	[O II]		3728.837	4.3 ± 0.1	20.1 ± 0.2	13.9488 ± 0.1260	110.7	0.0390 ± 0.0091	C
		?	3728.261	-42.1 ± 0.1	28.3 ± 0.0	0.5447 ± 0.1267	4.3		
3734.368	H I		3734.360	-0.6 ± 0.2	26.0 ± 0.4	1.0729 ± 0.0153	69.9	0.1621 ± 0.0170	
			3733.842	-42.2 ± 1.3	34.1 ± 3.6	0.1739 ± 0.0181	9.6		
3750.151	H I		3750.142	-0.7 ± 0.2	26.7 ± 0.3	1.3333 ± 0.0179	74.4	0.1452 ± 0.0104	C
			3749.620	-42.5 ± 0.2	28.3 ± 0.0	0.1936 ± 0.0136	14.2		
3770.630	H I		3770.625	-0.4 ± 0.1	26.5 ± 0.2	2.3596 ± 0.0252	93.6	0.1216 ± 0.0110	avg
			3770.095	-42.5 ± 0.8	28.0 ± 2.3	0.2869 ± 0.0258	11.1		
3781.942	Fe I	?	3781.933	-0.7 ± 2.0	13.8 ± 4.9	0.0114 ± 0.0039	2.9	···	S
			···	···	···	···	···		
3784.895	He I		3784.841	-4.3 ± 1.1	14.3 ± 2.8	0.0211 ± 0.0038	5.5	0.2986 ± 0.1197	small FWHM
		?	3784.513	-30.2 ± 1.0	5.7 ± 2.1	0.0063 ± 0.0023	2.8		
3797.898	H I		3797.891	-0.6 ± 0.1	26.6 ± 0.2	2.2831 ± 0.0177	129.1	0.1532 ± 0.0081	
			3797.349	-43.3 ± 0.6	29.2 ± 1.5	0.3498 ± 0.0183	19.1		
3805.777	He I	?	3805.694	-6.5 ± 1.6	15.1 ± 4.0	0.0151 ± 0.0040	3.8	···	S
			···	···	···	···	···		
3806.526	Si III	?	3806.482	-3.4 ± 0.9	6.8 ± 1.9	0.0062 ± 0.0017	3.6	···	S small FWHM
			···	···	···	···	···		
3819.614	He I		3819.617	0.2 ± 0.2	21.9 ± 0.7	0.4219 ± 0.0132	32.0	0.1714 ± 0.0286	C
			3819.081	-41.9 ± 0.2	28.3 ± 0.0	0.0723 ± 0.0119	6.1		
3833.584	He I	?	3833.532	-4.0 ± 1.2	15.2 ± 3.0	0.0302 ± 0.0063	4.8	···	S
			···	···	···	···	···		
3835.384	H I		3835.379	-0.4 ± 0.1	27.2 ± 0.1	4.7665 ± 0.0289	164.7	0.1374 ± 0.0065	avg
			3834.830	-43.3 ± 0.5	28.4 ± 1.3	0.6550 ± 0.0309	21.2		
3837.726	S III	?	3837.787	4.7 ± 0.5	6.7 ± 1.3	0.0102 ± 0.0020	5.0	···	S small FWHM
			···	···	···	···	···		
3838.374	N II	?	3838.256	-9.2 ± 2.3	23.7 ± 6.9	0.0251 ± 0.0087	2.9	···	S
			···	···	···	···	···		
3856.018	Si II		3856.043	1.9 ± 0.5	20.4 ± 1.2	0.0791 ± 0.0048	16.6	0.2023 ± 0.0575	C
		?	3855.477	-42.1 ± 0.5	28.3 ± 0.0	0.0160 ± 0.0044	3.6		
3862.595	Si II		3862.621	2.0 ± 0.7	18.1 ± 1.7	0.0443 ± 0.0041	10.8	···	S
			···	···	···	···	···		
3867.472	He I		3867.495	1.8 ± 0.5	14.5 ± 1.4	0.0313 ± 0.0033	9.5	···	S
			···	···	···	···	···		
3868.750	[Ne III]		3868.740	-0.8 ± 0.1	14.0 ± 0.2	8.0485 ± 0.1063	75.7	0.2602 ± 0.0202	
			3868.204	-42.3 ± 0.8	25.4 ± 1.9	2.0946 ± 0.1599	13.1		
3871.790	He I		3871.781	-0.7 ± 0.5	15.4 ± 1.1	0.0370 ± 0.0027	13.8	0.3297 ± 0.0839	C
		?	3871.246	-42.2 ± 0.5	28.3 ± 0.0	0.0122 ± 0.0030	4.1		
3889.049	H I		3889.009	-3.1 ± 0.7	32.8 ± 1.8	6.9463 ± 0.4236	16.4	0.1773 ± 0.0392	C , He I line blend
		?	3888.517	-41.0 ± 0.7	28.3 ± 0.0	1.2317 ± 0.2621	4.7		
3918.968	C II		3918.934	-2.6 ± 0.8	15.3 ± 1.9	0.0243 ± 0.0028	8.6	0.4362 ± 0.1416	C
		?	3918.417	-42.2 ± 0.8	28.3 ± 0.0	0.0106 ± 0.0032	3.3		
3920.681	C II		3920.627	-4.1 ± 0.3	14.4 ± 0.8	0.0490 ± 0.0026	18.5	···	S
			···	···	···	···	···		
3926.544	He I		3926.537	-0.5 ± 0.4	18.1 ± 0.9	0.0641 ± 0.0031	20.6	0.2699 ± 0.0508	C
			3925.991	-42.2 ± 0.4	28.3 ± 0.0	0.0173 ± 0.0031	5.5		
3928.556	S III	?	3928.567	0.8 ± 1.8	10.8 ± 4.4	0.0070 ± 0.0027	2.6	···	S
			···	···	···	···	···		
3935.945	He I	?	3935.945	0.0 ± 0.8	5.5 ± 2.7	0.0043 ± 0.0014	3.1	···	S small FWHM
			···	···	···	···	···		
···		?	3952.737	···	13.7 ± 5.2	0.0075 ± 0.0028	2.7	···	S
			···	···	···	···	···		
3964.728	He I		3964.726	-0.2 ± 0.1	17.4 ± 0.3	0.5317 ± 0.0079	67.4	0.1332 ± 0.0158	C avg
			3964.171	-42.1 ± 0.1	28.3 ± 0.0	0.0708 ± 0.0083	8.5		
3967.460	[Ne III]		3967.442	-1.4 ± 0.1	14.5 ± 0.1	3.9684 ± 0.0354	112.0	0.2311 ± 0.0134	avg
			3966.891	-43.0 ± 0.5	24.2 ± 1.2	0.9172 ± 0.0527	17.4		
3970.072	H I		3970.067	-0.4 ± 0.1	26.4 ± 0.1	11.8942 ± 0.0700	170.0	0.1372 ± 0.0069	avg
			3969.510	-42.5 ± 0.4	28.7 ± 1.2	1.6322 ± 0.0816	20.0		

Table 1—Continued

ID Wave[a,b] (1)	ID (2)	?[c] (3)	Wavel[d] (4)	Velocity[e] (5)	FWHM[e,f] (6)	I_{corr}[g,h] (7)	S/N[i] (8)	I_{sh}/I_{neb}[j] (9)	Notes[k] (10)
3993.059	[Ni II]	?	3993.258	15.0 ± 1.6	9.9 ± 3.8	0.0069 ± 0.0025	2.8	···	S small FWHM
			···	···	···	···	···		
4008.350	[Fe III]		4008.332	-1.4 ± 0.7	9.5 ± 1.6	0.0115 ± 0.0019	6.2	···	S small FWHM
			···	···	···	···	···		
4009.256	He I		4009.256	-0.0 ± 0.2	15.7 ± 0.6	0.0684 ± 0.0025	27.4	···	S
			···	···	···	···	···		
4023.980	He I	?	4023.934	-3.4 ± 1.5	12.7 ± 3.6	0.0086 ± 0.0023	3.7	···	S
			···	···	···	···	···		
4026.184	He I		4026.201	1.3 ± 0.2	19.0 ± 0.6	1.0062 ± 0.0303	33.2	0.2282 ± 0.0308	C
			4025.622	-41.9 ± 0.2	28.3 ± 0.0	0.2296 ± 0.0302	7.6		
4068.600	[S II]		4068.700	7.3 ± 0.1	18.6 ± 0.2	0.7661 ± 0.0076	101.1	0.0470 ± 0.0094	C
		?	4068.031	-41.9 ± 0.1	28.3 ± 0.0	0.0360 ± 0.0072	5.0		
4069.882	O II	?	4069.805	-5.7 ± 1.9	28.7 ± 5.4	0.0306 ± 0.0067	4.6	···	S
			···	···	···	···	···		
4072.153	O II		4072.148	-0.3 ± 0.4	13.1 ± 1.1	0.0269 ± 0.0022	12.1	0.2937 ± 0.1077	C
		?	4071.582	-42.1 ± 0.4	28.3 ± 0.0	0.0079 ± 0.0028	2.8		
4075.862	O II		4075.851	-0.8 ± 0.3	14.8 ± 0.9	0.0407 ± 0.0033	12.2	0.2211 ± 0.0640	
		?	4075.292	-41.9 ± 1.4	15.7 ± 4.0	0.0090 ± 0.0025	3.6		
4076.350	[S II]		4076.454	7.7 ± 0.1	17.7 ± 0.3	0.2393 ± 0.0045	53.6	···	S
			···	···	···	···	···		
4079.700	[Fe III]	?	4079.659	-3.0 ± 1.0	8.1 ± 2.5	0.0051 ± 0.0015	3.5	···	S small FWHM
			···	···	···	···	···		
4083.899	O II	?	4083.854	-3.3 ± 1.5	9.8 ± 3.5	0.0052 ± 0.0017	3.0	···	S small FWHM
			···	···	···	···	···		
4085.112	O II	?	4085.105	-0.5 ± 2.2	20.5 ± 5.7	0.0097 ± 0.0027	3.6	···	S
			···	···	···	···	···		
4089.288	O II	?	4089.285	-0.2 ± 1.6	11.6 ± 4.0	0.0085 ± 0.0027	3.1	···	S
			···	···	···	···	···		
4092.929	O II	?	4092.915	-1.0 ± 0.8	6.8 ± 2.3	0.0060 ± 0.0017	3.6	···	S small FWHM
			···	···	···	···	···		
4097.225	O II	?	4097.184	-3.0 ± 3.4	30.7 ± 9.7	0.0243 ± 0.0093	2.6	···	S , O II line blend
			···	···	···	···	···		
4101.734	H I		4101.734	0.0 ± 0.1	27.2 ± 0.2	15.5127 ± 0.1098	141.3	0.1306 ± 0.0066	avg
			4101.188	-39.9 ± 0.5	24.2 ± 1.3	2.0266 ± 0.1008	20.1		
4110.786	O II	?	4110.750	-2.7 ± 1.5	9.1 ± 3.6	0.0071 ± 0.0025	2.8	···	S small FWHM
			···	···	···	···	···		
4116.104	Si IV	?	4116.225	8.8 ± 0.9	7.2 ± 2.0	0.0038 ± 0.0011	3.6	···	S small FWHM
			···	···	···	···	···		
4119.217	O II		4119.198	-1.4 ± 0.9	11.7 ± 2.1	0.0122 ± 0.0020	6.0	0.7377 ± 0.2825	
		?	4118.714	-36.6 ± 3.2	23.2 ± 8.0	0.0090 ± 0.0031	2.9		
4120.811	He I		4120.817	0.5 ± 0.3	19.7 ± 0.8	0.0854 ± 0.0033	25.9	0.2927 ± 0.0387	C
			4120.231	-42.1 ± 0.3	28.3 ± 0.0	0.0250 ± 0.0032	7.9		
4121.463	O II	?	4121.508	3.3 ± 0.7	8.4 ± 1.9	0.0054 ± 0.0012	4.4	···	S small FWHM
			···	···	···	···	···		
4132.800	O II		4132.729	-5.2 ± 1.0	14.3 ± 2.6	0.0112 ± 0.0020	5.6	···	S
			···	···	···	···	···		
4143.759	He I		4143.755	-0.3 ± 0.2	18.0 ± 0.5	0.1402 ± 0.0036	38.7	0.1277 ± 0.0263	C
		?	4143.178	-42.0 ± 0.2	28.3 ± 0.0	0.0179 ± 0.0037	4.9		
4153.298	O II		4153.279	-1.3 ± 0.5	15.9 ± 1.2	0.0214 ± 0.0016	13.6	0.5234 ± 0.0904	C
			4152.714	-42.1 ± 0.5	28.3 ± 0.0	0.0112 ± 0.0017	6.4		
4156.530	O II		4156.315	-15.5 ± 0.5	9.0 ± 1.2	0.0096 ± 0.0012	8.0	···	S small FWHM
			···	···	···	···	···		
4168.972	He I	?	4168.990	1.3 ± 1.7	21.6 ± 4.4	0.0175 ± 0.0036	4.9	···	S
			···	···	···	···	···		
4185.440	O II	?	4185.431	-0.6 ± 1.1	11.8 ± 2.6	0.0112 ± 0.0023	4.8	···	S
			···	···	···	···	···		
4189.788	O II	?	4189.756	-2.3 ± 1.1	5.6 ± 2.2	0.0046 ± 0.0017	2.7	···	S , O II line blend
			···	···	···	···	···		
4241.246	Cl II	?	4241.432	13.1 ± 1.4	17.2 ± 3.7	0.0115 ± 0.0026	4.5	···	S
			···	···	···	···	···		
4243.969	[Fe II]		4244.144	12.4 ± 0.4	16.2 ± 0.8	0.0308 ± 0.0015	20.0	···	S
			···	···	···	···	···		
4248.799	[Ni II]		4249.030	16.3 ± 0.9	13.2 ± 2.2	0.0072 ± 0.0012	6.2	···	S
			···	···	···	···	···		
4267.001	C II		4267.167	11.6 ± 0.6	28.2 ± 1.8	0.1069 ± 0.0076	14.1	···	S avg , C II line blend
			···	···	···	···	···		

Table 1—Continued

ID Wave[a,b] (1)	ID (2)	?[c] (3)	Wavel[d] (4)	Velocity[e] (5)	FWHM[e,f] (6)	I_{corr}[g,h] (7)	S/N[i] (8)	I_{sh}/I_{neb}[j] (9)	Notes[k] (10)
4275.551	O II	?	4275.568	1.2 ± 2.4	17.9 ± 6.2	0.0083 ± 0.0030	2.8	···	S
			···	···	···	···	···		
4276.749	O II		4277.003	17.8 ± 1.2	18.6 ± 3.0	0.0177 ± 0.0028	6.3	···	S
			···	···	···	···	···		
4287.727	O II		4287.570	-11.0 ± 0.2	13.4 ± 0.6	0.0411 ± 0.0018	23.4	···	S
			···	···	···	···	···		
4303.611	O II		4303.783	12.0 ± 1.3	24.4 ± 3.9	0.0110 ± 0.0018	6.1	0.7182 ± 0.1836	C , O II line blend
		?	4303.021	-41.1 ± 1.3	28.3 ± 0.0	0.0079 ± 0.0015	5.1		
4314.290	Fe II	?	4314.193	-6.7 ± 1.7	14.8 ± 4.4	0.0069 ± 0.0020	3.4	···	S
			···	···	···	···	···		
4317.139	O II		4317.081	-4.0 ± 1.0	13.5 ± 2.4	0.0090 ± 0.0015	6.0	···	S
			···	···	···	···	···		
4326.237	[Ni II]		4326.462	15.6 ± 0.6	10.7 ± 1.5	0.0129 ± 0.0017	7.5	···	S
			···	···	···	···	···		
4332.653	S III	?	4332.708	3.8 ± 1.6	17.5 ± 4.1	0.0078 ± 0.0019	4.2	···	S
			···	···	···	···	···		
4336.859	O II	?	4336.951	6.4 ± 2.6	19.0 ± 6.6	0.0077 ± 0.0028	2.8	···	S
			···	···	···	···	···		
4340.464	H I		4340.463	-0.0 ± 0.0	27.1 ± 0.1	26.7320 ± 0.1459	183.2	0.1656 ± 0.0059	avg
			4339.850	-42.4 ± 0.4	29.1 ± 1.1	4.4261 ± 0.1570	28.2		
4345.560	O II		4345.523	-2.5 ± 0.7	12.9 ± 1.8	0.0191 ± 0.0023	8.3	0.7225 ± 0.1796	C avg , O II line blend
		?	4344.944	-42.5 ± 0.7	28.3 ± 0.0	0.0138 ± 0.0030	4.6		
4349.426	O II		4349.389	-2.5 ± 1.1	17.0 ± 2.8	0.0183 ± 0.0028	6.6	···	S avg
			···	···	···	···	···		
4352.778	[Fe II]	?	4352.932	10.6 ± 1.0	13.4 ± 2.7	0.0078 ± 0.0016	4.9	···	S
			···	···	···	···	···		
4359.333	[Fe II]		4359.523	13.0 ± 0.3	11.7 ± 0.6	0.0268 ± 0.0014	19.6	···	S
			···	···	···	···	···		
4363.209	[O III]		4363.197	-0.8 ± 0.1	14.9 ± 0.2	0.5331 ± 0.0073	73.5	0.2990 ± 0.0219	
			4362.627	-40.0 ± 1.0	32.8 ± 2.5	0.1594 ± 0.0115	13.9		
4366.895	O II	?	4366.849	-3.1 ± 1.6	19.4 ± 4.1	0.0110 ± 0.0023	4.8	0.6364 ± 0.2444	C
		?	4366.265	-43.2 ± 1.6	28.3 ± 0.0	0.0070 ± 0.0023	3.1		
4368.193	O I		4368.448	17.5 ± 0.3	13.5 ± 0.6	0.0331 ± 0.0015	21.9	···	S , O I line blend
			···	···	···	···	···		
4387.929	He I		4387.925	-0.3 ± 0.1	19.2 ± 0.2	0.2463 ± 0.0026	93.1	0.1750 ± 0.0134	
			4387.323	-41.4 ± 0.9	27.7 ± 2.3	0.0431 ± 0.0033	13.2		
4391.995	Ne II	?	4391.896	-6.7 ± 1.6	20.3 ± 4.2	0.0083 ± 0.0017	4.9	···	S
			···	···	···	···	···		
4413.781	[Fe II]		4413.963	12.4 ± 0.5	15.9 ± 1.3	0.0241 ± 0.0020	11.9	···	S
			···	···	···	···	···		
4414.899	O II		4414.895	-0.3 ± 0.5	12.1 ± 1.3	0.0125 ± 0.0013	9.8	···	S
			···	···	···	···	···		
4416.266	[Fe II]		4416.441	11.9 ± 0.3	13.5 ± 1.0	0.0284 ± 0.0025	11.4	···	S
			···	···	···	···	···		
4425.437	Ca I	?	4425.578	9.6 ± 2.0	12.9 ± 5.0	0.0040 ± 0.0015	2.7	···	S
			···	···	···	···	···		
4437.554	He I		4437.568	0.9 ± 0.6	20.4 ± 1.5	0.0373 ± 0.0031	11.9	···	S avg
			···	···	···	···	···		
4452.378	O II		4452.293	-5.7 ± 0.5	13.8 ± 1.1	0.0169 ± 0.0013	12.6	0.2189 ± 0.0667	
		?	4451.910	-31.5 ± 1.4	10.7 ± 3.5	0.0037 ± 0.0011	3.4		
4457.945	[Fe II]		4458.151	13.9 ± 1.4	23.4 ± 3.7	0.0140 ± 0.0023	6.1	···	S
			···	···	···	···	···		
4465.407	O II	?	4465.357	-3.3 ± 1.7	18.9 ± 4.4	0.0074 ± 0.0017	4.4	···	S
			···	···	···	···	···		
4471.489	He I		4471.492	0.2 ± 0.1	20.7 ± 0.4	1.9679 ± 0.0359	54.8	0.1637 ± 0.0229	
			4470.874	-41.3 ± 1.4	26.8 ± 3.7	0.3221 ± 0.0447	7.2		
4474.904	[Fe II]	?	4475.097	13.0 ± 1.1	10.4 ± 3.0	0.0053 ± 0.0017	3.1	···	S
			···	···	···	···	···		
4514.900	[Fe II]	?	4515.015	7.6 ± 2.1	17.1 ± 5.3	0.0058 ± 0.0018	3.3	···	S
			···	···	···	···	···		
4571.096	Mg I]	?	4571.182	5.6 ± 2.9	19.0 ± 7.3	0.0038 ± 0.0015	2.6	···	S
			···	···	···	···	···		
4590.974	O II		4590.960	-0.9 ± 1.0	17.4 ± 2.5	0.0104 ± 0.0014	7.2	0.4423 ± 0.1597	C
		?	4590.325	-42.4 ± 1.0	28.3 ± 0.0	0.0046 ± 0.0015	3.0		
4596.177	O II	?	4596.120	-3.7 ± 0.8	10.0 ± 2.5	0.0055 ± 0.0015	3.6	···	S
			···	···	···	···	···		

Table 1—Continued

ID Wave[a,b] (1)	ID (2)	?[c] (3)	Wavel[d] (4)	Velocity[e] (5)	FWHM[e,f] (6)	I_{corr}[g,h] (7)	S/N[i] (8)	I_{sh}/I_{neb}[j] (9)	Notes[k] (10)
4596.840	[Ni III]	?	4597.071	15.1 ± 1.2	7.5 ± 3.1	0.0028 ± 0.0011	2.6	···	S small FWHM
			···	···	···	···	···		
4607.030	[Fe III]		4607.102	4.7 ± 0.5	17.7 ± 1.3	0.0303 ± 0.0021	14.3	0.2508 ± 0.0780	C
		?	4606.383	-42.1 ± 0.5	28.3 ± 0.0	0.0076 ± 0.0023	3.3		
4609.436	O II	?	4609.386	-3.3 ± 1.2	7.6 ± 2.8	0.0056 ± 0.0019	2.9	···	S small FWHM
			···	···	···	···	···		
4621.418	Si II	?	4621.186	-15.1 ± 2.4	23.1 ± 6.1	0.0087 ± 0.0022	3.9	···	S
			···	···	···	···	···		
4630.539	N II		4630.539	-0.0 ± 0.8	17.7 ± 2.0	0.0197 ± 0.0022	9.0	0.5685 ± 0.1321	C
		?	4629.893	-41.9 ± 0.8	28.3 ± 0.0	0.0112 ± 0.0023	4.9		
4634.130	N III	?	4634.073	-3.7 ± 1.1	7.6 ± 2.6	0.0032 ± 0.0011	3.0	···	S small FWHM
			···	···	···	···	···		
4638.856	O II		4638.830	-1.7 ± 0.7	16.0 ± 1.7	0.0184 ± 0.0019	9.8	0.4620 ± 0.1247	C
		?	4638.200	-42.4 ± 0.7	28.3 ± 0.0	0.0085 ± 0.0021	4.0		
4641.810	O II		4641.803	-0.5 ± 0.3	13.8 ± 0.6	0.0320 ± 0.0012	25.7	0.2625 ± 0.0480	C
			4641.159	-42.1 ± 0.3	28.3 ± 0.0	0.0084 ± 0.0015	5.6		
4643.086	N II	?	4643.102	1.1 ± 0.9	10.3 ± 2.2	0.0049 ± 0.0010	5.1	···	S
			···	···	···	···	···		
4649.135	O II		4649.126	-0.5 ± 0.2	15.1 ± 0.5	0.0524 ± 0.0016	32.2	0.4046 ± 0.0554	
			4648.520	-39.7 ± 1.6	33.4 ± 4.4	0.0212 ± 0.0028	7.5		
4650.838	O II		4650.828	-0.7 ± 0.4	14.9 ± 1.0	0.0186 ± 0.0011	16.5	0.4516 ± 0.0825	C
			4650.184	-42.2 ± 0.4	28.3 ± 0.0	0.0084 ± 0.0014	5.8		
4658.050	[Fe III]		4658.156	6.8 ± 0.1	16.9 ± 0.3	0.3503 ± 0.0062	56.9	0.1818 ± 0.0211	
			4657.476	-36.9 ± 1.0	21.6 ± 2.5	0.0637 ± 0.0073	8.7		
4661.632	O II		4661.629	-0.2 ± 0.3	14.6 ± 0.6	0.0206 ± 0.0009	23.5	0.2087 ± 0.0435	
		?	4660.854	-50.1 ± 1.3	15.1 ± 3.2	0.0043 ± 0.0009	4.9		
4667.010	[Fe III]		4667.049	2.5 ± 0.7	16.9 ± 1.9	0.0101 ± 0.0011	9.4	0.2079 ± 0.0728	small FWHM
		?	4666.347	-42.6 ± 1.3	8.7 ± 3.1	0.0021 ± 0.0007	3.0		
4676.235	O II		4676.206	-1.9 ± 0.6	15.9 ± 1.5	0.0152 ± 0.0014	11.2	0.2895 ± 0.1031	C
		?	4675.574	-42.4 ± 0.6	28.3 ± 0.0	0.0044 ± 0.0015	2.9		
4699.011	O II	?	4699.181	10.8 ± 2.4	17.8 ± 5.9	0.0046 ± 0.0015	3.1	···	S , O II line blend
			···	···	···	···	···		
4701.530	[Fe III]		4701.606	4.9 ± 0.1	15.7 ± 0.3	0.1157 ± 0.0024	48.1	0.1867 ± 0.0242	
			4700.926	-38.5 ± 1.0	18.8 ± 2.4	0.0216 ± 0.0028	7.8		
4705.346	O II	?	4705.353	0.4 ± 1.3	10.5 ± 3.3	0.0066 ± 0.0019	3.5	···	S
			···	···	···	···	···		
4711.370	[Ar IV]		4711.325	-2.9 ± 0.4	13.4 ± 1.0	0.0241 ± 0.0017	14.6	···	S avg
			···	···	···	···	···		
4713.139	He I		4713.171	2.1 ± 0.2	19.6 ± 0.5	0.2593 ± 0.0065	39.9	0.1465 ± 0.0243	C
			4712.486	-41.5 ± 0.2	28.3 ± 0.0	0.0380 ± 0.0062	6.1		
4733.910	[Fe III]		4733.943	2.1 ± 0.3	16.2 ± 0.6	0.0430 ± 0.0015	28.9	0.1651 ± 0.0317	
			4733.280	-39.9 ± 1.1	14.2 ± 2.8	0.0071 ± 0.0013	5.3		
4740.170	[Ar IV]		4740.195	1.6 ± 0.3	14.5 ± 0.6	0.0281 ± 0.0011	24.6	0.2954 ± 0.0491	C
			4739.505	-42.1 ± 0.3	28.3 ± 0.0	0.0083 ± 0.0013	6.2		
4754.690	[Fe III]		4754.782	5.8 ± 0.2	17.4 ± 0.5	0.0654 ± 0.0019	34.0	0.2064 ± 0.0349	
			4754.122	-35.8 ± 1.6	24.3 ± 4.1	0.0135 ± 0.0023	6.0		
4769.430	[Fe III]		4769.508	4.9 ± 0.3	18.0 ± 0.6	0.0394 ± 0.0013	30.8	0.3096 ± 0.0442	
			4768.825	-38.1 ± 1.3	26.4 ± 3.5	0.0122 ± 0.0017	7.2		
4777.680	[Fe III]		4777.757	4.8 ± 0.3	15.6 ± 0.8	0.0213 ± 0.0011	20.1	0.2535 ± 0.0631	
		?	4777.096	-36.6 ± 2.2	21.9 ± 5.5	0.0054 ± 0.0013	4.1		
4779.722	N II	?	4779.733	0.7 ± 1.3	13.1 ± 3.2	0.0039 ± 0.0009	4.2	···	S
			···	···	···	···	···		
4788.138	N II	?	4788.157	1.2 ± 1.1	12.3 ± 2.8	0.0041 ± 0.0009	4.7	···	S
			···	···	···	···	···		
4814.534	[Fe II]		4814.751	13.5 ± 0.6	13.5 ± 1.6	0.0232 ± 0.0030	7.8	···	S avg
			···	···	···	···	···		
4861.325	H I		4861.332	0.4 ± 0.1	27.6 ± 0.2	38.6262 ± 0.2739	141.0	0.1548 ± 0.0070	
			4860.634	-42.6 ± 0.6	29.2 ± 1.4	5.9776 ± 0.2657	22.5		
4867.120	N III		4867.098	-1.4 ± 1.5	26.2 ± 4.1	0.0069 ± 0.0011	6.1	···	S
			···	···	···	···	···		
4881.000	[Fe III]		4881.079	4.8 ± 0.2	16.3 ± 0.4	0.1588 ± 0.0038	41.5	0.1858 ± 0.0265	
			4880.359	-39.4 ± 1.0	18.5 ± 2.6	0.0295 ± 0.0042	7.1		
4889.617	[Fe II]		4889.846	14.0 ± 0.5	13.6 ± 1.2	0.0140 ± 0.0012	11.7	···	S
			···	···	···	···	···		
4895.117	N II		4894.899	-13.3 ± 1.9	29.5 ± 5.2	0.0097 ± 0.0019	5.2	0.4948 ± 0.1816	
		?	4894.148	-59.3 ± 2.9	24.5 ± 7.5	0.0048 ± 0.0015	3.2		

Table 1—Continued

ID Wave[a,b] (1)	ID (2)	?[c] (3)	Wavel[d] (4)	Velocity[e] (5)	FWHM[e,f] (6)	I_{corr}[g,h] (7)	S/N[i] (8)	I_{sh}/I_{neb}[j] (9)	Notes[k] (10)
4905.339	[Fe II]		4905.535	12.0 ± 0.8	10.1 ± 1.9	0.0052 ± 0.0009	5.6	···	S
			···	···	···	···	···		
4921.931	He I		4921.937	0.4 ± 0.1	18.1 ± 0.2	0.5355 ± 0.0055	97.0	0.2256 ± 0.0164	avg
			4921.278	-39.8 ± 0.8	32.8 ± 2.3	0.1208 ± 0.0087	13.9		
4924.529	O II		4924.537	0.5 ± 1.3	18.4 ± 3.6	0.0126 ± 0.0024	5.2	0.7460 ± 0.2391	C , [Fe III] line blend
		?	4923.850	-41.3 ± 1.3	28.3 ± 0.0	0.0094 ± 0.0024	3.9		
4930.540	[Fe III]	?	4930.642	6.2 ± 1.6	24.1 ± 5.4	0.0154 ± 0.0050	3.1	···	S
			···	···	···	···	···		
4931.227	[O III]		4931.236	0.6 ± 0.5	12.9 ± 1.4	0.0176 ± 0.0020	8.8	···	S
			···	···	···	···	···		
4947.373	[Fe II]		4947.573	12.1 ± 1.0	11.4 ± 2.4	0.0069 ± 0.0013	5.2	···	S
			···	···	···	···	···		
4958.911	[O III]		4958.923	0.7 ± 0.1	14.7 ± 0.2	49.5053 ± 0.6134	80.7	0.2714 ± 0.0191	
			4958.247	-40.2 ± 0.8	27.7 ± 2.0	13.4351 ± 0.9330	14.4		
4985.900	[Fe III]		4985.901	0.1 ± 1.2	20.2 ± 3.0	0.0097 ± 0.0015	6.6	···	S
			···	···	···	···	···		
4987.376	N II		4987.294	-4.9 ± 0.2	15.5 ± 0.6	0.0301 ± 0.0012	25.8	···	S , [Fe III] line blend
			···	···	···	···	···		
5006.843	[O III]		5006.846	0.2 ± 0.1	14.4 ± 0.1	145.5834 ± 1.3295	109.5	0.3030 ± 0.0130	
			5006.155	-41.2 ± 0.5	26.4 ± 1.2	44.1151 ± 1.8458	23.9		
5011.260	[Fe III]		5011.338	4.7 ± 0.7	15.0 ± 1.8	0.0430 ± 0.0048	8.9	0.5814 ± 0.1531	C
		?	5010.569	-41.3 ± 0.7	28.3 ± 0.0	0.0250 ± 0.0060	4.2		
5015.678	He I		5015.677	-0.1 ± 0.1	17.7 ± 0.2	1.0266 ± 0.0143	72.0	0.1669 ± 0.0189	
			5014.994	-40.9 ± 1.1	26.5 ± 2.9	0.1713 ± 0.0192	8.9		
5035.399	[Fe II]		5035.653	15.1 ± 1.3	27.9 ± 3.5	0.0449 ± 0.0062	7.3	···	S
			···	···	···	···	···		
5041.024	Si II		5041.055	1.8 ± 0.4	16.9 ± 1.1	0.0413 ± 0.0027	15.5	0.4189 ± 0.0738	C
			5040.320	-41.9 ± 0.4	28.3 ± 0.0	0.0173 ± 0.0028	6.1		
5047.738	He I		5047.761	1.4 ± 0.4	18.8 ± 0.9	0.0785 ± 0.0038	20.5	0.2242 ± 0.0489	C
		?	5047.031	-42.0 ± 0.4	28.3 ± 0.0	0.0176 ± 0.0037	4.7		
5055.984	Si II		5056.038	3.2 ± 0.4	22.2 ± 1.0	0.0924 ± 0.0045	20.6	0.1364 ± 0.0431	C
		?	5055.277	-41.9 ± 0.4	28.3 ± 0.0	0.0126 ± 0.0039	3.2		
5084.770	[Fe III]		5084.826	3.3 ± 1.1	21.3 ± 3.0	0.0083 ± 0.0012	7.1	0.4819 ± 0.1438	C
		?	5084.046	-42.7 ± 1.1	28.3 ± 0.0	0.0040 ± 0.0011	3.8		
5111.627	[Fe II]		5111.862	13.8 ± 0.3	7.5 ± 0.7	0.0057 ± 0.0005	11.6	···	B S small FWHM
			···	···	···	···	···		
5146.749	Co I		5146.894	8.5 ± 1.2	16.4 ± 2.8	0.0136 ± 0.0023	5.9	···	B S
			···	···	···	···	···		
5146.749	Co I		5146.904	9.0 ± 0.9	17.4 ± 2.3	0.0141 ± 0.0017	8.4	···	R S
			···	···	···	···	···		
5158.777	[Fe II]		5158.996	12.7 ± 0.3	17.3 ± 0.8	0.0330 ± 0.0015	21.9	0.1455 ± 0.0506	B C
		?	5158.052	-42.1 ± 0.3	28.3 ± 0.0	0.0048 ± 0.0017	2.9		
5158.777	[Fe II]		5159.001	13.0 ± 0.5	18.0 ± 1.2	0.0283 ± 0.0017	16.5	···	R S
			···	···	···	···	···		
5169.033	Fe II	?	5169.334	17.4 ± 3.8	36.8 ± 11.0	0.0078 ± 0.0029	2.7	···	B S
			···	···	···	···	···		
5169.033	Fe II	?	5169.274	14.0 ± 0.6	6.3 ± 1.5	0.0040 ± 0.0008	4.9	···	R S small FWHM
			···	···	···	···	···		
5191.816	[Ar III]	?	5191.497	-18.4 ± 3.5	27.8 ± 9.2	0.0373 ± 0.0129	2.9	···	R S
			···	···	···	···	···		
5197.902	[N I]		5198.161	14.9 ± 0.1	12.3 ± 0.3	0.0624 ± 0.0014	43.6	···	B S
			···	···	···	···	···		
5197.902	[N I]	?	5198.172	15.6 ± 0.2	10.0 ± 0.8	0.0361 ± 0.0075	4.8	0.6051 ± 0.2140	R
		?	5198.125	12.9 ± 1.2	20.2 ± 2.8	0.0218 ± 0.0062	3.5		
5200.257	[N I]		5200.509	14.6 ± 0.2	13.2 ± 0.4	0.0415 ± 0.0011	38.1	···	B S
			···	···	···	···	···		
5200.257	[N I]		5200.513	14.8 ± 0.2	11.9 ± 0.6	0.0294 ± 0.0015	20.1	···	R S
			···	···	···	···	···		
5219.307	S III	?	5219.332	1.4 ± 1.1	10.2 ± 2.8	0.0019 ± 0.0005	3.8	···	B S
			···	···	···	···	···		
5220.059	[Fe II]	?	5220.305	14.1 ± 2.0	24.2 ± 5.3	0.0046 ± 0.0011	4.1	···	B S
			···	···	···	···	···		
5220.059	[Fe II]	?	5219.961	-5.6 ± 1.6	10.4 ± 3.9	0.0035 ± 0.0013	2.7	···	R S
			···	···	···	···	···		
5261.621	[Fe II]		5261.868	14.0 ± 0.5	12.9 ± 1.2	0.0280 ± 0.0025	11.4	···	B S
			···	···	···	···	···		

Table 1—Continued

ID Wave[a,b] (1)	ID (2)	?[c] (3)	Wavel[d] (4)	Velocity[e] (5)	FWHM[e,f] (6)	I_{corr}[g,h] (7)	S/N[i] (8)	I_{sh}/I_{neb}[j] (9)	Notes[k] (10)
5261.621	[Fe II]		5261.869	14.1 ± 0.3	13.7 ± 0.8	0.0208 ± 0.0012	17.2	···	R S
			···	···	···	···	···		
5270.400	[Fe III]		5270.550	8.5 ± 0.1	17.0 ± 0.3	0.1677 ± 0.0029	57.5	0.2218 ± 0.0232	B avg
			5269.821	−32.9 ± 1.1	25.6 ± 2.9	0.0372 ± 0.0038	9.7		
5270.400	[Fe III]		5270.555	8.8 ± 0.1	16.1 ± 0.3	0.1595 ± 0.0028	56.6	0.2329 ± 0.0212	R
			5269.840	−31.9 ± 1.1	27.6 ± 2.7	0.0371 ± 0.0033	11.2		
5273.346	[Fe II]		5273.624	15.8 ± 0.7	13.9 ± 1.9	0.0128 ± 0.0016	7.9	···	B S
			···	···	···	···	···		
5273.346	[Fe II]		5273.592	14.0 ± 0.6	15.7 ± 1.5	0.0138 ± 0.0014	9.7	···	R S avg
			···	···	···	···	···		
5275.123	O I	?	5275.411	16.3 ± 1.6	24.3 ± 4.8	0.0087 ± 0.0023	3.8	···	R S avg , O I line blend
			···	···	···	···	···		
5299.044	O I		5299.241	11.1 ± 0.4	15.0 ± 1.0	0.0134 ± 0.0009	15.7	···	B S , O I line blend
			···	···	···	···	···		
5299.044	O I		5299.260	12.2 ± 0.7	15.5 ± 1.9	0.0094 ± 0.0011	8.7	···	R S , O I line blend
			···	···	···	···	···		
5333.646	[Fe II]		5333.886	13.5 ± 0.6	13.4 ± 1.5	0.0061 ± 0.0006	9.6	···	B S
			···	···	···	···	···		
5333.646	[Fe II]	?	5333.876	13.0 ± 1.5	13.9 ± 3.5	0.0066 ± 0.0015	4.3	···	R S
			···	···	···	···	···		
···		?	5342.423	···	14.5 ± 3.0	0.0065 ± 0.0015	4.4	···	R S avg
			···	···	···	···	···		
···		?	5342.426	···	14.2 ± 4.0	0.0035 ± 0.0009	3.7	···	B S
			···	···	···	···	···		
5363.340	[Ni IV]	?	5363.676	18.8 ± 0.8	7.4 ± 2.0	0.0021 ± 0.0005	4.2	···	B S small FWHM
			···	···	···	···	···		
5363.340	[Ni IV]	?	5363.625	15.9 ± 2.3	26.1 ± 5.9	0.0052 ± 0.0011	4.6	0.2615 ± 0.1093	R small FWHM
		?	5362.970	−20.7 ± 1.5	8.9 ± 3.6	0.0014 ± 0.0005	2.8		
5376.452	[Fe II]	?	5376.693	13.4 ± 1.3	15.0 ± 3.2	0.0048 ± 0.0010	4.9	···	B S
			···	···	···	···	···		
5376.452	[Fe II]	?	5376.672	12.3 ± 2.0	16.4 ± 4.9	0.0030 ± 0.0008	3.8	···	R S avg
			···	···	···	···	···		
5411.980	[Fe III]		5412.167	10.4 ± 0.4	12.8 ± 1.0	0.0150 ± 0.0011	13.9	0.2667 ± 0.1043	B
		?	5411.265	−39.6 ± 3.0	20.8 ± 7.9	0.0040 ± 0.0015	2.6		
5411.980	[Fe III]		5412.162	10.1 ± 0.5	14.6 ± 1.2	0.0134 ± 0.0010	12.8	···	R S
			···	···	···	···	···		
5433.129	[Fe II]	?	5433.386	14.2 ± 1.2	13.6 ± 2.9	0.0046 ± 0.0010	4.8	···	B S
			···	···	···	···	···		
5453.855	S II	?	5453.855	0.0 ± 2.3	16.3 ± 5.7	0.0027 ± 0.0009	2.9	···	B S
			···	···	···	···	···		
5495.655	N II	?	5495.596	−3.2 ± 1.7	13.4 ± 4.3	0.0027 ± 0.0008	3.4	···	B S
			···	···	···	···	···		
5495.655	N II	?	5495.675	1.1 ± 0.6	7.1 ± 4.2	0.0024 ± 0.0005	4.7	···	R S avg small FWHM
			···	···	···	···	···		
5512.772	O I		5512.988	11.8 ± 1.0	13.6 ± 2.5	0.0091 ± 0.0016	5.7	···	B S , O I line blend
			···	···	···	···	···		
5512.772	O I		5512.977	11.2 ± 0.8	21.4 ± 1.8	0.0119 ± 0.0009	12.9	···	R S , O I line blend
			···	···	···	···	···		
5517.720	[Cl III]		5517.686	−1.9 ± 0.2	15.6 ± 0.4	0.1582 ± 0.0040	39.4	0.1195 ± 0.0286	B C
		?	5516.948	−42.0 ± 0.2	28.3 ± 0.0	0.0189 ± 0.0045	4.2		
5517.720	[Cl III]		5517.697	−1.3 ± 0.2	14.9 ± 0.5	0.1284 ± 0.0038	33.8	0.1609 ± 0.0296	R C
			5516.925	−43.2 ± 0.2	28.3 ± 0.0	0.0207 ± 0.0038	5.5		
5518.102	N I		5518.360	14.0 ± 0.6	9.9 ± 1.6	0.0098 ± 0.0018	5.6	···	B S small FWHM
			···	···	···	···	···		
5518.102	N I	?	5518.250	8.0 ± 1.4	26.6 ± 4.1	0.0190 ± 0.0037	5.1	···	R S
			···	···	···	···	···		
···		?	5527.516	···	16.9 ± 5.5	0.0029 ± 0.0009	3.4	···	R S
			···	···	···	···	···		
5537.890	[Cl III]		5537.863	−1.5 ± 0.1	18.8 ± 0.2	0.2170 ± 0.0023	95.9	0.2005 ± 0.0129	B
			5537.118	−41.8 ± 0.7	26.0 ± 1.8	0.0435 ± 0.0028	15.8		
5537.890	[Cl III]		5537.849	−2.2 ± 0.1	16.0 ± 0.2	0.2139 ± 0.0024	90.6	0.1915 ± 0.0136	R avg
			5537.071	−44.4 ± 0.8	27.8 ± 2.1	0.0410 ± 0.0029	14.3		
5551.922	N II		5551.862	−3.2 ± 0.9	11.4 ± 2.2	0.0033 ± 0.0006	5.3	···	R S avg
			···	···	···	···	···		
5555.004	O I		5555.228	12.1 ± 0.5	17.9 ± 1.2	0.0123 ± 0.0008	14.7	···	B S , O I line blend
			···	···	···	···	···		

Table 1—Continued

ID Wave[a,b] (1)	ID (2)	?[c] (3)	Wavel[d] (4)	Velocity[e] (5)	FWHM[e,f] (6)	I_{corr}[g,h] (7)	S/N[i] (8)	I_{sh}/I_{neb}[j] (9)	Notes[k] (10)
5555.004	O I		5555.219	11.6 ± 0.6	19.0 ± 1.4	0.0119 ± 0.0008	14.9	···	R S , O I line blend
			···	···	···	···	···		
5577.339	[O I]		5577.607	14.4 ± 0.8	16.3 ± 2.2	0.0046 ± 0.0007	6.7	···	B S
			···	···	···	···	···		
5577.339	[O I]	?	5577.611	14.6 ± 0.7	8.8 ± 1.7	0.0039 ± 0.0008	4.7	···	R S avg small FWHM
			···	···	···	···	···		
5606.151	S II	?	5606.186	1.9 ± 1.5	9.7 ± 3.6	0.0015 ± 0.0005	2.9	···	B S small FWHM
			···	···	···	···	···		
5666.630	N II		5666.613	-0.9 ± 0.9	21.4 ± 2.2	0.0115 ± 0.0011	10.2	0.2957 ± 0.0850	R C
		?	5665.827	-42.5 ± 0.9	28.3 ± 0.0	0.0034 ± 0.0009	3.7		
5676.020	N II	?	5676.053	1.7 ± 1.4	15.1 ± 3.3	0.0063 ± 0.0015	4.1	···	R S avg
			···	···	···	···	···		
5679.560	N II		5679.578	0.9 ± 1.2	24.9 ± 3.0	0.0177 ± 0.0022	8.0	···	B S
			···	···	···	···	···		
5679.560	N II		5679.551	-0.5 ± 0.4	17.2 ± 0.9	0.0171 ± 0.0009	20.0	0.1342 ± 0.0468	R C
		?	5678.749	-42.8 ± 0.4	28.3 ± 0.0	0.0023 ± 0.0008	2.9		
5686.210	N II	?	5686.020	-10.0 ± 2.3	28.0 ± 6.3	0.0051 ± 0.0012	4.4	0.5333 ± 0.1827	R C
		?	5685.222	-52.1 ± 2.3	28.3 ± 0.0	0.0027 ± 0.0007	3.9		
5710.770	N II	?	5710.778	0.4 ± 0.8	5.7 ± 1.5	0.0014 ± 0.0004	3.6	···	B S small FWHM
			···	···	···	···	···		
5710.770	N II		5710.775	0.3 ± 0.6	11.6 ± 1.5	0.0047 ± 0.0006	8.1	0.4160 ± 0.1572	R C
		?	5709.956	-42.7 ± 0.6	28.3 ± 0.0	0.0020 ± 0.0007	2.8		
5739.730	Si III		5739.687	-2.3 ± 0.7	14.4 ± 1.8	0.0056 ± 0.0007	8.4	0.5536 ± 0.1565	B C
		?	5738.923	-42.2 ± 0.7	28.3 ± 0.0	0.0031 ± 0.0008	3.9		
5739.730	Si III		5739.731	0.1 ± 0.7	9.7 ± 1.8	0.0036 ± 0.0006	5.7	0.8736 ± 0.2625	R C small FWHM
		?	5738.907	-43.0 ± 0.7	28.3 ± 0.0	0.0031 ± 0.0008	4.1		
5754.590	[N II]		5754.724	7.0 ± 0.1	19.9 ± 0.2	0.3248 ± 0.0028	117.1	0.0443 ± 0.0084	B C
			5753.784	-42.0 ± 0.1	28.3 ± 0.0	0.0144 ± 0.0027	5.3		
5754.590	[N II]		5754.735	7.6 ± 0.1	20.1 ± 0.2	0.3225 ± 0.0034	95.1	0.0448 ± 0.0090	R C
		?	5753.769	-42.8 ± 0.1	28.3 ± 0.0	0.0145 ± 0.0029	5.0		
5867.600	Al II	?	5867.875	14.0 ± 1.4	11.4 ± 3.3	0.0027 ± 0.0007	3.8	0.8148 ± 0.3534	B
		?	5866.962	-32.6 ± 1.9	12.5 ± 4.7	0.0022 ± 0.0008	2.9		
5875.640	He I		5875.652	0.6 ± 0.2	23.7 ± 0.3	5.7619 ± 0.0713	80.8	0.1604 ± 0.0130	B
			5874.831	-41.3 ± 0.9	25.3 ± 2.3	0.9243 ± 0.0739	12.5		
5875.640	He I		5875.648	0.4 ± 0.2	21.6 ± 0.3	5.7021 ± 0.0735	77.6	0.1686 ± 0.0124	R
			5874.833	-41.2 ± 0.9	26.7 ± 2.2	0.9616 ± 0.0697	13.8		
···			5887.613	···	14.2 ± 2.4	0.0048 ± 0.0008	6.2	···	B S
			···	···	···	···	···		
5889.280	C II		5889.334	2.8 ± 0.3	13.1 ± 0.7	0.0160 ± 0.0011	15.2	···	B S
			···	···	···	···	···		
···		?	5906.023	···	28.3 ± 6.1	0.0054 ± 0.0012	4.6	0.2593 ± 0.1113	B small FWHM
		?	5905.154	···	8.1 ± 3.2	0.0014 ± 0.0005	2.7		
5927.810	N II	?	5927.791	-1.0 ± 1.6	12.3 ± 3.8	0.0021 ± 0.0006	3.5	···	R S
			···	···	···	···	···		
5931.780	N II	?	5931.848	3.5 ± 1.1	7.1 ± 2.5	0.0028 ± 0.0009	3.0	···	B S small FWHM
			···	···	···	···	···		
5931.780	N II		5931.942	8.2 ± 1.7	29.2 ± 4.6	0.0102 ± 0.0016	6.2	···	R S
			···	···	···	···	···		
5952.390	N II	?	5952.523	6.7 ± 1.4	15.2 ± 3.3	0.0050 ± 0.0011	4.7	···	R S
			···	···	···	···	···		
5957.560	Si II		5957.739	9.0 ± 0.5	23.0 ± 1.8	0.0187 ± 0.0020	9.3	···	R S avg
			···	···	···	···	···		
5958.386	O I		5958.831	22.4 ± 0.3	18.4 ± 0.9	0.0146 ± 0.0007	19.6	···	R S avg , O I line blend
			···	···	···	···	···		
5978.930	Si II		5979.095	8.3 ± 0.5	24.6 ± 1.1	0.0464 ± 0.0021	22.4	···	S avg
			···	···	···	···	···		
6046.438	O I		6046.681	12.1 ± 0.2	18.5 ± 0.5	0.0406 ± 0.0010	39.0	···	S , O I line blend
			···	···	···	···	···		
6300.304	[O I]		6300.578	13.0 ± 0.1	15.1 ± 0.1	0.3954 ± 0.0035	112.1	0.0413 ± 0.0098	C avg
		?	6299.405	-42.8 ± 0.1	28.3 ± 0.0	0.0163 ± 0.0039	4.2		sky line
6312.060	[S III]		6312.105	2.1 ± 0.1	17.0 ± 0.2	0.7587 ± 0.0076	99.9	0.2105 ± 0.0121	avg
			6311.234	-39.2 ± 0.7	29.3 ± 1.8	0.1597 ± 0.0090	17.7		
6347.110	Si II		6347.181	3.3 ± 0.3	22.6 ± 0.9	0.0798 ± 0.0030	26.8	0.1651 ± 0.0282	C
			6346.199	-43.0 ± 0.3	28.3 ± 0.0	0.0132 ± 0.0022	6.0		
6363.776	[O I]		6364.053	13.0 ± 0.1	14.7 ± 0.2	0.1273 ± 0.0018	72.1	···	S avg
			···	···	···	···	···		

Table 1—Continued

ID Wave[a,b] (1)	ID (2)	?[c] (3)	Wavel[d] (4)	Velocity[e] (5)	FWHM[e,f] (6)	I_{corr}[g,h] (7)	S/N[i] (8)	I_{sh}/I_{neb}[j] (9)	Notes[k] (10)
6365.100	[Ni II]		6365.468	17.3 ± 1.0	13.4 ± 2.6	0.0033 ± 0.0006	5.3	···	S
			···	···	···	···	···		
6371.370	Si II		6371.419	2.3 ± 0.2	21.0 ± 0.6	0.0389 ± 0.0010	37.3	0.1683 ± 0.0203	C avg
			6370.463	-42.7 ± 0.2	28.3 ± 0.0	0.0065 ± 0.0008	8.5		
6401.500	[Ni III]	?	6401.221	-13.1 ± 0.9	6.1 ± 1.8	0.0014 ± 0.0004	3.6	···	S small FWHM
			···	···	···	···	···		
6402.246	Ne I	?	6402.275	1.3 ± 0.9	10.7 ± 2.3	0.0014 ± 0.0003	4.7	···	S
			···	···	···	···	···		
6440.400	[Fe II]	?	6440.342	-2.7 ± 0.6	6.2 ± 1.4	0.0019 ± 0.0004	4.6	···	S small FWHM
			···	···	···	···	···		
···			6461.834	···	16.8 ± 0.9	0.0097 ± 0.0005	17.9	0.1856 ± 0.0475	
		?	6460.851	···	13.9 ± 3.7	0.0018 ± 0.0004	4.0		
6533.800	[Ni III]		6533.607	-8.8 ± 0.8	12.4 ± 2.0	0.0057 ± 0.0009	6.6	···	S
			···	···	···	···	···		
6548.050	[N II]		6548.211	7.4 ± 0.1	20.4 ± 0.1	6.4136 ± 0.0317	202.1	0.0347 ± 0.0041	C avg
			6547.117	-42.7 ± 0.1	28.3 ± 0.0	0.2225 ± 0.0265	8.4		
···			6550.283	···	25.2 ± 3.0	0.0725 ± 0.0091	8.0	···	S
			···	···	···	···	···		
6562.800	H I		6562.834	1.6 ± 0.0	28.0 ± 0.1	123.2699 ± 0.4158	296.5	0.1769 ± 0.0031	avg
			6561.914	-40.5 ± 0.3	32.0 ± 0.6	21.8084 ± 0.3741	58.3		
6578.050	C II		6578.039	-0.5 ± 0.2	14.5 ± 0.4	0.0647 ± 0.0020	33.1	0.0920 ± 0.0318	
		?	6577.052	-45.5 ± 1.7	15.1 ± 4.8	0.0060 ± 0.0021	2.9		
6583.450	[N II]		6583.584	6.1 ± 0.1	20.3 ± 0.1	19.8713 ± 0.1009	197.0	0.0396 ± 0.0042	C avg
			6582.510	-42.8 ± 0.1	28.3 ± 0.0	0.7870 ± 0.0837	9.4		
6666.800	[Ni II]		6667.141	15.3 ± 0.3	12.0 ± 0.7	0.0064 ± 0.0003	18.3	···	S avg
			···	···	···	···	···		
6678.152	He I		6678.170	0.8 ± 0.1	18.5 ± 0.1	1.5329 ± 0.0118	129.9	0.1997 ± 0.0088	avg
			6677.276	-39.3 ± 0.6	29.8 ± 1.4	0.3061 ± 0.0133	23.1		
6682.200	[Ni III]	?	6681.962	-10.7 ± 1.0	9.3 ± 2.5	0.0017 ± 0.0004	3.8	···	S avg small FWHM
			···	···	···	···	···		
6716.440	[S II]		6716.625	8.3 ± 0.1	22.9 ± 0.2	1.1012 ± 0.0094	117.5	0.0266 ± 0.0065	C
		?	6715.480	-42.9 ± 0.1	28.3 ± 0.0	0.0292 ± 0.0071	4.1		
6730.816	[S II]		6731.013	8.8 ± 0.0	21.2 ± 0.1	1.9971 ± 0.0123	162.4	0.0294 ± 0.0049	C
			6729.855	-42.8 ± 0.0	28.3 ± 0.0	0.0587 ± 0.0098	6.0		
6739.800	[Fe IV]		6739.771	-1.3 ± 0.4	10.7 ± 1.0	0.0061 ± 0.0005	12.2	···	S
			···	···	···	···	···		
6747.500	[Cr IV]		6747.609	4.9 ± 0.8	15.4 ± 2.2	0.0043 ± 0.0006	7.3	0.4942 ± 0.1497	C
		?	6746.542	-42.5 ± 0.8	28.3 ± 0.0	0.0021 ± 0.0006	3.7		
6813.570	[Ni II]		6813.961	17.2 ± 0.7	9.1 ± 1.6	0.0022 ± 0.0003	6.5	···	S small FWHM
			···	···	···	···	···		
···		?	6826.557	···	9.7 ± 2.2	0.0027 ± 0.0006	4.6	···	S small FWHM
			···	···	···	···	···		
···			6861.664	···	14.1 ± 1.9	0.0030 ± 0.0004	7.8	···	S
			···	···	···	···	···		
···		?	6890.575	···	35.1 ± 12.1	0.0160 ± 0.0057	2.8	0.8375 ± 0.3595	C
		?	6889.606	···	28.3 ± 0.0	0.0134 ± 0.0032	4.2		
6906.436	O II	?	6906.431	-0.2 ± 1.1	12.2 ± 2.9	0.0023 ± 0.0005	4.2	···	S
			···	···	···	···	···		
6915.200	[Cr IV]	?	6915.431	10.0 ± 1.3	11.0 ± 3.4	0.0018 ± 0.0006	3.0	···	S
			···	···	···	···	···		
6933.890	He I		6933.980	3.9 ± 0.7	14.1 ± 1.8	0.0051 ± 0.0006	8.3	···	S avg
			···	···	···	···	···		
6946.400	[Ni III]	?	6946.115	-12.3 ± 1.4	13.2 ± 3.9	0.0025 ± 0.0008	3.0	···	S
			···	···	···	···	···		
6989.450	He I	?	6989.658	8.9 ± 1.2	11.9 ± 3.0	0.0018 ± 0.0004	4.2	···	S
			···	···	···	···	···		
7002.173	O I		7002.476	13.0 ± 0.3	25.8 ± 0.7	0.0443 ± 0.0012	36.1	···	S avg , O I line blend
			···	···	···	···	···		
7062.260	He I		7062.306	1.9 ± 1.1	15.5 ± 2.7	0.0041 ± 0.0007	5.7	···	S
			···	···	···	···	···		
7065.179	He I		7065.223	1.9 ± 0.1	20.1 ± 0.3	2.7998 ± 0.0389	72.0	0.1346 ± 0.0137	avg
			7064.248	-39.5 ± 1.2	25.9 ± 3.0	0.3768 ± 0.0381	9.9		
···		?	7080.442	···	13.2 ± 3.7	0.0018 ± 0.0005	3.8	···	S
			···	···	···	···	···		
7135.790	[Ar III]		7135.797	0.3 ± 0.1	14.8 ± 0.2	6.3300 ± 0.0690	91.7	0.2609 ± 0.0142	
			7134.900	-37.4 ± 0.9	36.0 ± 2.3	1.6518 ± 0.0883	18.7		

Table 1—Continued

ID Wave[a,b] (1)	ID (2)	?[c] (3)	Wavel[d] (4)	Velocity[e] (5)	FWHM[e,f] (6)	I_{corr}[g,h] (7)	S/N[i] (8)	I_{sh}/I_{neb}[j] (9)	Notes[k] (10)
7155.160	[Fe II]		7155.429	11.3 ± 0.4	19.2 ± 1.0	0.0305 ± 0.0016	18.5	···	S
			···	···	···	···	···		
7160.580	He I		7160.578	-0.1 ± 0.4	17.9 ± 1.1	0.0107 ± 0.0006	16.5	0.2701 ± 0.0554	C
		?	7159.558	-42.8 ± 0.4	28.3 ± 0.0	0.0029 ± 0.0006	5.1		
7172.000	[Fe II]	?	7172.187	7.8 ± 1.1	10.0 ± 2.8	0.0042 ± 0.0011	3.7	···	S
			···	···	···	···	···		
7231.330	C II		7231.380	2.1 ± 0.9	14.6 ± 2.2	0.0144 ± 0.0020	7.1	0.5194 ± 0.1655	C
		?	7230.290	-43.1 ± 0.9	28.3 ± 0.0	0.0075 ± 0.0021	3.5		
7236.420	C II		7236.440	0.8 ± 0.2	15.1 ± 0.6	0.0503 ± 0.0020	25.3	···	S
			···	···	···	···	···		
7254.448	O I		7254.724	11.4 ± 0.4	24.0 ± 0.9	0.0601 ± 0.0023	26.5	0.1188 ± 0.0300	C avg , O I line blend
		?	7253.405	-43.1 ± 0.4	28.3 ± 0.0	0.0071 ± 0.0018	4.0		
7281.351	He I		7281.408	2.3 ± 0.1	21.7 ± 0.3	0.2218 ± 0.0032	70.1	0.2453 ± 0.0147	avg
			7280.441	-37.5 ± 0.8	32.0 ± 2.1	0.0544 ± 0.0032	17.2		
7298.030	He I		7298.039	0.4 ± 0.5	22.7 ± 1.4	0.0214 ± 0.0015	14.4	0.2304 ± 0.0441	C
			7297.002	-42.2 ± 0.5	28.3 ± 0.0	0.0049 ± 0.0009	5.6		
7319.073	[O II]		7319.203	5.3 ± 0.2	23.8 ± 0.6	0.9192 ± 0.0204	45.1	0.0541 ± 0.0169	T
		?	7318.044	-42.1 ± 0.2	28.3 ± 0.0	0.0497 ± 0.0155	3.2		
7320.157	[O II]		7320.271	4.7 ± 0.1	20.3 ± 0.2	1.9687 ± 0.0182	107.9	···	T
			···	···	···	···	···		
7329.699	[O II]		7329.821	5.0 ± 0.2	26.0 ± 0.4	1.0801 ± 0.0150	71.8	0.0933 ± 0.0100	T
			7328.669	-42.1 ± 0.2	28.3 ± 0.0	0.1007 ± 0.0107	9.4		
7330.786	[O II]		7330.906	4.9 ± 0.1	20.9 ± 0.3	1.0964 ± 0.0134	82.0	···	T
			···	···	···	···	···		
7377.830	[Ni II]		7378.183	14.3 ± 0.1	17.2 ± 0.3	0.0402 ± 0.0007	54.8	···	S avg
			···	···	···	···	···		
7388.180	[Fe II]		7388.446	10.8 ± 1.1	24.4 ± 3.0	0.0061 ± 0.0008	8.1	···	S
			···	···	···	···	···		
7411.610	[Ni II]	?	7411.910	12.1 ± 1.3	12.4 ± 3.6	0.0141 ± 0.0043	3.3	···	S
			···	···	···	···	···		
7423.641	N I		7424.035	15.9 ± 0.4	13.3 ± 0.9	0.0067 ± 0.0004	15.9	···	S
			···	···	···	···	···		
7468.312	N I		7468.687	15.0 ± 0.2	11.9 ± 0.4	0.0183 ± 0.0006	32.5	···	S
			···	···	···	···	···		

[a]ID wavelength of line, in air. Wavelengths are from the Atomic Line List v2.04 (http://www.pa.uky.edu/~peter/atomic/, maintained by P. A. M. van Hoof), except O II (Blagrave & Martin 2004).

[b]Nebular (neb) and shock (sh) components are included in separate, consecutive rows for each ID wavelength. If there is no shock component, the second row is left blank. Lines with no identification are included, but Columns (1), (2) and (5) are left blank.

[c]A low S/N ($2.6 < S/N < 5.2$) is flagged with a '?'

[d]Observed wavelength of line peak adjusted to rest frame of nebular H^+ as defined by median of first six unblended H I Balmer lines

[e]km s^{-1}

[f]A quoted FWHM of 28.3 ± 0.0 is the result of a constrained double Gaussian fit.

[g]Reddening-corrected surface brightness (I_{corr}, 10^{-13} ergs cm^{-2} s^{-1} $arcsec^{-2}$) and its uncertainty calculated from the best-fit Gaussian area and its 68.3% confidence interval.

[h]The red shock lines have been adjusted by a factor of 0.85 to correct for slit coverage differences between the red and blue spectra. The nebular lines are not adjusted.

[i]Signal-to-noise from surface brightness and 68.3% confidence interval.

[j]The shock-to-nebula ratio is entered within the 'nebula' row and the 'shock' row is left blank.

[k]Constrained double Gaussian fit (C), constrained triple Gaussian fit (T), single Gaussian fit (S), red echelle spectrum (R), blue echelle spectrum (B), average of two orders (avg).

Table 2. Blue/red echelle spectra comparison.

ID Wave (1)	ID (2)	Wavel (3)	Velocity (4)	FWHM (5)	I_{obs}[a] (6)	S/N (7)	B/R[b] (8)	Notes (9)
5270.400	[Fe III]	5270.550	8.5 ± 0.1	17.0 ± 0.3	0.0248	57.5	1.051 ± 0.026	B avg
		5269.821	-32.9 ± 1.1	25.6 ± 2.9	0.0055	9.7	0.846 ± 0.115	
5270.400	[Fe III]	5270.555	8.8 ± 0.1	16.1 ± 0.3	0.0236	56.6	···	R
		5269.840	-31.9 ± 1.1	27.6 ± 2.7	0.0065	11.2	···	
5517.720	[Cl III]	5517.686	-1.9 ± 0.2	15.6 ± 0.4	0.0250	39.4	1.232 ± 0.048	B C
		5516.948	-42.0 ± 0.2	28.3 ± 0.0	0.0030	4.2	0.789 ± 0.237	
5517.720	[Cl III]	5517.697	-1.3 ± 0.2	14.9 ± 0.5	0.0203	33.8	···	R C
		5516.925	-43.2 ± 0.2	28.3 ± 0.0	0.0038	5.5	···	
5537.890	[Cl III]	5537.863	-1.5 ± 0.1	18.8 ± 0.2	0.0345	95.9	1.015 ± 0.015	B
		5537.118	-41.8 ± 0.7	26.0 ± 1.8	0.0069	15.8	0.896 ± 0.085	
5537.890	[Cl III]	5537.849	-2.2 ± 0.1	16.0 ± 0.2	0.0340	90.6	···	R avg
		5537.071	-44.4 ± 0.8	27.8 ± 2.1	0.0077	14.3	···	
5739.730	Si III	5739.687	-2.3 ± 0.7	14.4 ± 1.8	0.0009	8.4	1.500 ± 0.318	B C
		5738.923	-42.2 ± 0.7	28.3 ± 0.0	0.0005	3.9	0.833 ± 0.295	
5739.730	Si III	5739.731	0.1 ± 0.7	9.7 ± 1.8	0.0006	5.7	···	R C
		5738.907	-43.0 ± 0.7	28.3 ± 0.0	0.0006	4.1	···	
5754.590	[N II]	5754.724	7.0 ± 0.1	19.9 ± 0.2	0.0545	117.1	1.006 ± 0.014	B C
		5753.784	-42.0 ± 0.1	28.3 ± 0.0	0.0024	5.3	0.828 ± 0.228	
5754.590	[N II]	5754.735	7.6 ± 0.1	20.1 ± 0.2	0.0542	95.1	···	R C
		5753.769	-42.8 ± 0.1	28.3 ± 0.0	0.0029	5.0	···	
5875.640	He I	5875.652	0.6 ± 0.2	23.7 ± 0.3	0.9977	80.8	1.010 ± 0.018	B
		5874.831	-41.3 ± 0.9	25.3 ± 2.3	0.1600	12.5	0.817 ± 0.088	
5875.640	He I	5875.648	0.4 ± 0.2	21.6 ± 0.3	0.9874	77.6	···	R
		5874.833	-41.2 ± 0.9	26.7 ± 2.2	0.1959	13.8	···	

[a] 10^{-13} ergs cm^{-2} s^{-1} arcsec^{-2}, before reddening correction

[b] The blue/red ratio (B/R) is entered in the 'blue' rows for the nebula (1st row) and the shock (2nd row). The 'red' rows are left blank.

Table 3. Physical conditions within the nebula and the shock

Parameter	Line	Nebula	Shock
N_e (cm^{-3})	[S II][a]	5896^{+404}_{-366}	13183^{+10000}_{-11183}
	[O II][b]	1939^{+50}_{-50}	2898^{+8429}_{-1997}
	[O II][c]	3811^{+50}_{-50}	7304^{+8429}_{-1997}
	[Fe III][d]	4700^{+800}_{-800}	7300^{+8000}_{-4100}
	[Cl III][e]	12074^{+1300}_{-1118}	21715^{+39170}_{-9641}
	[Cl III][f]	7247^{+575}_{-519}	10911^{+7515}_{-3665}
	O II[g]	6700^{+100}_{-100}	···
T_e (K)	[O I][h]	8005^{+580}_{-408}	···
	[N II][i]	10672^{+53}_{-52}	8784^{+1184}_{-729}
	[O III][j]	8536^{+35}_{-33}	8366^{+252}_{-214}

[a]A: Keenan et al. (1993) cs: Ramsbottom et al. (1996)

[b]A: Wiese et al. (1996) cs: McLaughlin & Bell (1993)

[c]A: Zeippen (1982) cs: McLaughlin & Bell (1993)

[d]Weighted average from 11 [Fe III] lines, following Keenan et al. (2001)

[e]A: Kaufman & Sugar (1986) cs: Ramsbottom et al. (1999)

[f]A: Mendoza & Zeippen (1982) cs: Ramsbottom et al. (1999)

[g]Following Peimbert & Peimbert (2005)

[h]A: Wiese et al. (1996) cs: Bhatia & Kastner (1995)

[i]A: Wiese et al. (1996) cs: Lennon & Burke (1994)

[j]A: Wiese et al. (1996) cs: Lennon & Burke (1994)

Table 4. O^{++}/H^+ ratios from permitted lines.

Transition	Lines (Å)	Nebula I_{sum}[a] ($\times 10^{-2}$)	Nebula O^{++}/H^+ ($\times 10^{-5}$) A[b]	Nebula O^{++}/H^+ ($\times 10^{-5}$) B[c]	Shock I_{sum}[a] ($\times 10^{-2}$)	Shock O^{++}/H^+ ($\times 10^{-5}$) A[b]	Shock O^{++}/H^+ ($\times 10^{-5}$) B[c]
3s ^{4}P-3p ^{4}D^0	4642+76	0.4285 ± 0.0891	27 ± 6	26 ± 6	0.7381 ± 0.1961	47 ± 12	45 ± 12
	4649	0.4355 ± 0.0213	28 ± 1	27 ± 1	1.0491 ± 0.1525	67 ± 10	65 ± 10
	avg	0.4351 ± 0.0250	28 ± 2	27 ± 2	0.9318 ± 0.1689	60 ± 11	57 ± 11

[a]Determined following Peimbert & Peimbert (2005) (their equations 3 and 4) using $N_e(\mathrm{FL})^{neb} \sim 6000$, $N_e(\mathrm{FL})^{shock} \sim 10000$

[b]Case A O II recombination coefficients (Storey 1994)

[c]Case B O II recombination coefficients (Storey 1994)

Table 5. O/H from collisionally excited lines and recombination lines with a derived t^2 parameter.

		$12+\log(X^m/H^+)$		
	Feature	CELs[a]	RLs[b,c]	t^2
O^{++}	Nebula	8.37 ± 0.01	8.43 ± 0.03	0.009 ± 0.004
	Shock	8.69 ± 0.05	8.76 ± 0.08	0.010 ± 0.010
O^+	Nebula	7.78 ± 0.03	···	···
	Shock	7.72 ± 0.18	···	···
O^0	Nebula	6.19 ± 0.03	···	···
	Shock	···	···	···
O_{tot}	Nebula	8.47 ± 0.01	8.52 ± 0.03[d]	···
	Shock	8.73 ± 0.05	8.80 ± 0.08[d]	···

[a]collisionally excited lines

[b]recombination lines

[c]using case B effective recombination coefficients (Storey 1994)

[d]O^{++} recombination; O^+, O^0 collisionally excited lines

Table 6. Constraints on Model Parameters

Quantity	HH Shock		
	Obs	Mod A[a]	Mod B[b]
F(He I λ6678)[c]	0.31 ± 0.01	0.34	0.33
$\lambda5007/\lambda6678$[d]	144.13 ± 8.68	136.45	149.67
$\lambda5007/\lambda3726$[d]	35.35 ± 6.96	40.11	33.62
$\lambda6312/\lambda6725$[d]	1.816 ± 0.270	0.851	1.421
$(\lambda4959 + \lambda5007)/\lambda4363$[e]	361.02 ± 39.15	381.57	380.17
$(\lambda6548 + \lambda6583)/\lambda5755$[e]	69.88 ± 17.84	78.84	70.48
$\lambda6731/\lambda6716$[f]	2.01 ± 0.59	2.14	2.14
$\lambda3726/\lambda3729$[f]	2.29 ± 0.69	2.57	2.57
$\lambda5518/\lambda5538$[f]	0.50 ± 0.10	0.45	0.45

[a]Mihalas stellar atmosphere, CLOUDY H II abundances

[b]Kurucz stellar atmosphere, Esteban et al. (2004) abundances

[c]10^{-13} ergs cm^{-2} s^{-1} arcsec^{-2}

[d]Ionization indicator

[e]Temperature indicator

[f]Density indicator

Table 7. CLOUDY input parameters

Quantity	Shock Mod A[a]	Shock Mod B[b]
$T_{\rm star}$ (K)	35200	41200
logϕ(H)	12.700	12.800
radius (pc)	undef	undef
log$n_{\rm H}$(inner)	4.20	4.20
Constant	ρ	ρ
Grains	yes	yes
thickness (pc)	0.00396	0.00391

[a]Mihalas stellar atmosphere, CLOUDY H II abundances

[b]Kurucz stellar atmosphere, Esteban et al. (2004) abundances

Table 8. Model abundances relative to H (12+log(X/H))

Element (1)	Shock Mod A[a] (2)	Shock Mod B[b] (3)
He	10.98	10.98
C	8.48	8.42
N	7.85	7.73
O	8.60	8.65
Ne	7.78	8.05
S	7.00	7.22
Ar	6.48	6.62
Cl	5.00	5.46

[a]CLOUDY H II region abundances from Baldwin et al. (1991); Rubin et al. (1991); Osterbrock et al. (1992)

[b]Esteban et al. (2004) abundances

Table 9. Comparison of model predictions and observations.

ID	ID	HH Shock[a]		
Species	Wavelength	Obs	Mod A[b]	Mod B[c]
He I	3512.5	0.164 ± 0.051	0.039	0.039
He I	3587.3	0.455 ± 0.123	0.096	0.096
He I	3613.6	0.154 ± 0.041	0.130	0.111
He I	3634.2	0.138 ± 0.051	0.137	0.138
H I	3667.7	0.169 ± 0.030	0.251	0.172
H I	3671.5	0.190 ± 0.035	0.279	0.192
H I	3673.8	0.124 ± 0.028	0.313	0.215
H I	3676.4	0.203 ± 0.032	0.352	0.243
H I	3679.4	0.243 ± 0.028	0.398	0.276
H I	3682.8	0.192 ± 0.032	0.451	0.315
H I	3686.8	0.241 ± 0.036	0.515	0.363
H I	3691.6	0.362 ± 0.046	0.591	0.421
H I	3697.2	0.425 ± 0.077	0.682	0.493
H I	3703.9	0.370 ± 0.051	0.794	0.582
H I	3712.0	0.641 ± 0.139	0.544	0.405
[O II]	3726.0	4.078 ± 0.784	3.402	4.452
[O II]	3728.8	1.780 ± 0.414	1.325	1.735
H I	3734.4	0.568 ± 0.059	0.836	0.644
H I	3750.2	0.632 ± 0.044	1.047	0.826
H I	3770.6	0.937 ± 0.084	1.365	1.092
He I	3784.9	0.021 ± 0.007	0.011	0.011
H I	3797.9	1.143 ± 0.060	1.792	1.460
He I	3819.6	0.236 ± 0.039	0.340	0.340
H I	3835.4	2.140 ± 0.101	2.436	2.027
[Ne III]	3868.8	6.843 ± 0.522	6.980	5.895
He I	3871.8	0.040 ± 0.010	0.025	0.025
H I	3889.0	4.024 ± 0.856[d]	3.460	2.932
He I	3926.5	0.057 ± 0.010	0.035	0.035
He I	3964.7	0.231 ± 0.027	0.267	0.236
[Ne III]	3967.5	2.997 ± 0.172	2.104	1.777
H I	3970.1	5.332 ± 0.267	5.136	4.444
He I	4026.2	0.750 ± 0.099	0.621	0.622
[S II]	4068.6	0.118 ± 0.024	0.280	0.291
O II	4075.9	0.029 ± 0.008	0.070	0.076
H I	4101.7	6.621 ± 0.329	8.246	7.307

Table 9—Continued

ID	ID	HH Shock[a]		
Species	Wavelength	Obs	Mod A[b]	Mod B[c]
He I	4120.8	0.082 ± 0.010	0.059	0.058
He I	4143.8	0.059 ± 0.012	0.088	0.088
O II	4153.3	0.037 ± 0.006	0.015	0.017
H I	4340.5	14.460 ± 0.513[d]	14.587	13.148
[O III]	4363.2	0.521 ± 0.037	0.476	0.524
He I	4387.9	0.141 ± 0.011	0.161	0.161
He I	4471.5	1.052 ± 0.146	1.330	1.331
[Fe III]	4607.0	0.025 ± 0.007	0.015	0.016
O II	4650.8	0.027 ± 0.005	0.115	0.126
[Fe III]	4658.0	0.208 ± 0.024	0.219	0.230
[Fe III]	4667.0	0.007 ± 0.002	0.011	0.012
[Fe III]	4701.5	0.071 ± 0.009	0.090	0.095
He I	4713.1	0.124 ± 0.020	0.184	0.182
[Fe III]	4733.9	0.023 ± 0.004	0.040	0.042
[Ar IV]	4740.2	0.027 ± 0.004	0.114	0.025
[Fe III]	4754.7	0.044 ± 0.007	0.040	0.042
[Fe III]	4769.4	0.040 ± 0.005	0.030	0.032
[Fe III]	4777.7	0.018 ± 0.004	0.019	0.020
H I	4861.3	19.529 ± 0.868	30.658	27.996
[Fe III]	4881.0	0.096 ± 0.014	0.114	0.120
He I	4921.9	0.395 ± 0.028	0.348	0.348
[O III]	4958.9	43.893 ± 3.048	45.331	49.725
[O III]	5006.8	144.127 ± 6.030	136.448	149.673
[Fe III]	5011.3	0.082 ± 0.019	0.042	0.044
He I	5015.7	0.560 ± 0.063	0.680	0.616
He I	5047.7	0.058 ± 0.012	0.051	0.047
[Fe III]	5084.8	0.013 ± 0.003	0.007	0.007
[Fe II]	5158.8	0.016 ± 0.005[e]	0.003	0.002
[Fe III]	5270.4	0.121 ± 0.013[e]	0.137	0.144
[Fe III]	5270.4	0.121 ± 0.011[f]	···	···
[Fe III]	5412.0	0.013 ± 0.005[e]	0.012	0.013
[Cl III]	5517.7	0.062 ± 0.015[e]	0.045	0.141
[Cl III]	5517.7	0.068 ± 0.012[f]	···	···
[Cl III]	5537.9	0.142 ± 0.009[e]	0.100	0.311
[Cl III]	5537.9	0.134 ± 0.009[f]	···	···

Table 9—Continued

ID	ID	HH Shock[a]		
Species	Wavelength	Obs	Mod A[b]	Mod B[c]
[N II]	5754.6	0.047 ± 0.009[e]	0.070	0.025
[N II]	5754.6	0.047 ± 0.009[f]	···	···
He I	5875.6	3.020 ± 0.242[e]	3.775	3.783
He I	5875.6	3.142 ± 0.228[f]	···	···
[O I]	6300.3	0.053 ± 0.013	0.002	0.002
[S III]	6312.1	0.522 ± 0.029	0.485	0.842
[N II]	6548.0	0.727 ± 0.087	1.403	0.446
H I	6562.8	71.250 ± 1.222	88.254	81.460
[N II]	6583.5	2.571 ± 0.274	4.140	1.316
He I	6678.2	1.000 ± 0.043	1.000	1.000
[S II]	6716.4	0.096 ± 0.023	0.182	0.189
[S II]	6730.8	0.192 ± 0.032	0.388	0.404
He I	7065.2	1.231 ± 0.124	1.859	1.864
[Ar III]	7135.8	5.397 ± 0.289	5.361	8.111
He I	7160.6	0.009 ± 0.002	0.006	0.006
C II	7231.3	0.024 ± 0.007	0.001	0.001
He I	7281.4	0.178 ± 0.010	0.205	0.191
He I	7298.0	0.016 ± 0.003	0.009	0.009
[O II]	7319.1	0.163 ± 0.051	0.104	0.137
[O II]	7329.7	0.329 ± 0.035	0.172	0.225

[a]All fluxes are quoted relative to He I 6678. In the cases where lines were observed in both the red and the blue spectrum, the blue observations are listed first, and the model predictions are not repeated.

[b]Mihalas stellar atmosphere, CLOUDY H II abundances

[c]Kurucz stellar atmosphere, Esteban et al. (2004) abundances

[d]Measurement is a blend

[e]Blue echelle spectrum

[f]Red echelle spectrum

Table 10. Iron abundance and depletion in the Orion nebula and HH shock

Element	Nebula					Shock	
	B91[a]	R97[b]	E98[c]	E04[d]	CLOUDY[e]	Mod A	Mod B
Gas (Fe/H)	0.042e-4	0.0016e-4	0.026e-4	0.017e-4	0.03e-4	0.034e-4	0.0523e-4
Gas (12+log(Fe/H))	6.62	5.20	6.41	6.23	6.48	6.53	6.72
Depletion[f] (dex)	-0.88	-2.30	-1.08	-1.27	-1.02	-0.97	-0.78

[a]Baldwin et al. (1991)

[b]Rubin et al. (1997), noted to be an anomalously low Fe abundance

[c]Esteban et al. (1998)

[d]Esteban et al. (2004)

[e]CLOUDY H II region abundances from Baldwin et al. (1991); Rubin et al. (1991); Osterbrock et al. (1992)

[f]Relative to solar (7.50, Grevesse & Sauval (1999))

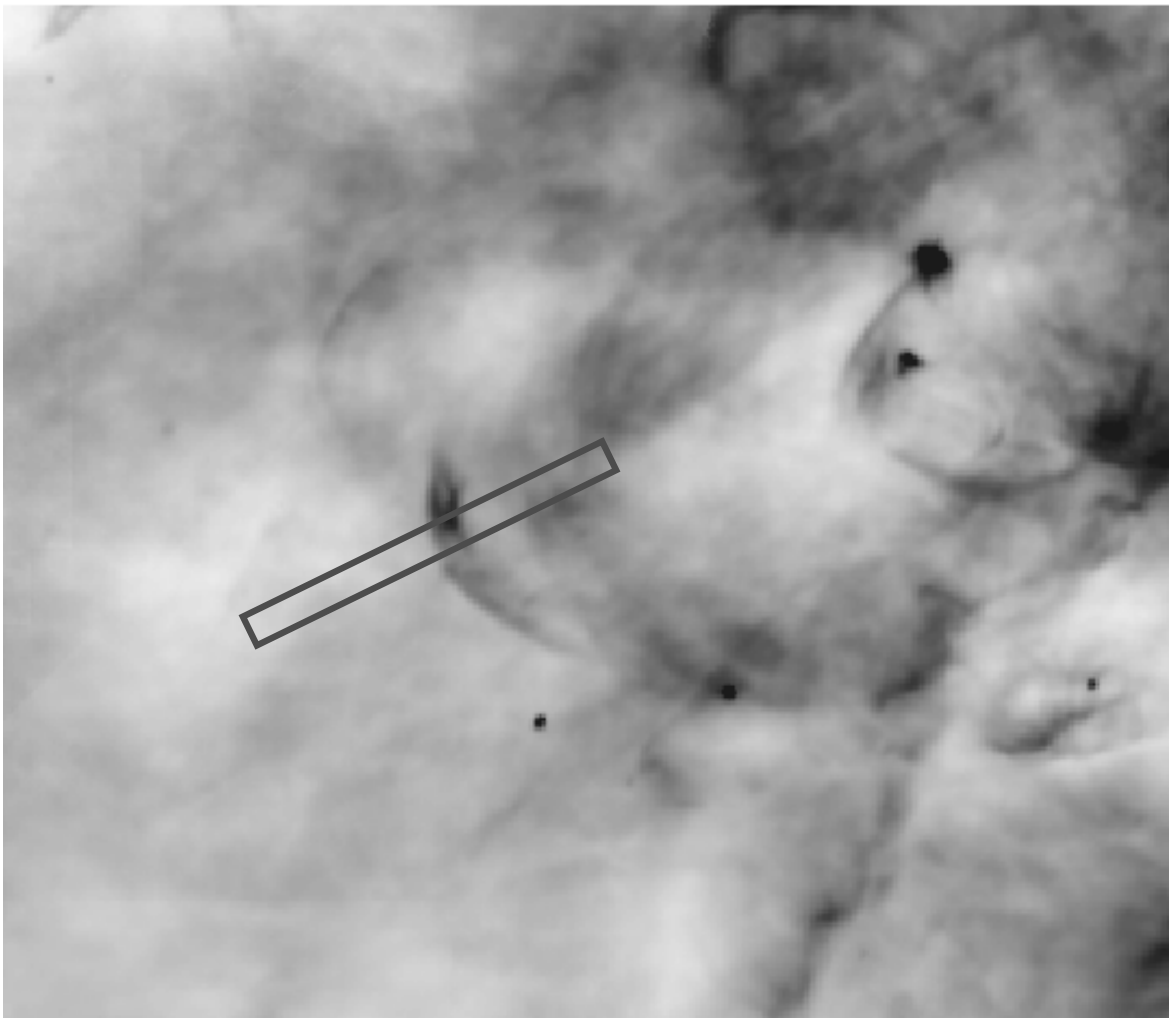

Fig. 1.— Red x2 slit position as determined from a Polaroid of the slit taken during observations, and the surface brightness variation across the slit as compared with the underlying F656N (Hα) WFPC2 image (O'Dell & Wong 1996). The slit is $12\farcs5 \times 1''$.

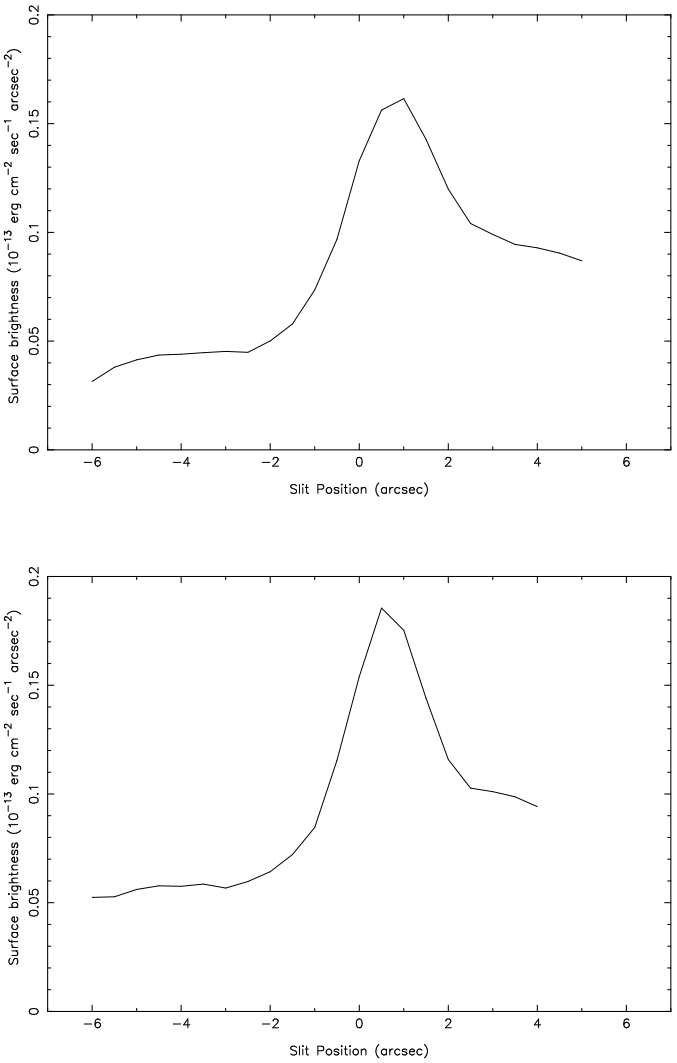

Fig. 2.— Flux variation of the He I 5876 spatially-narrow velocity-bridge component (+ continuum) along the slit in the blue spectrum (top) and in the red spectrum (bottom).

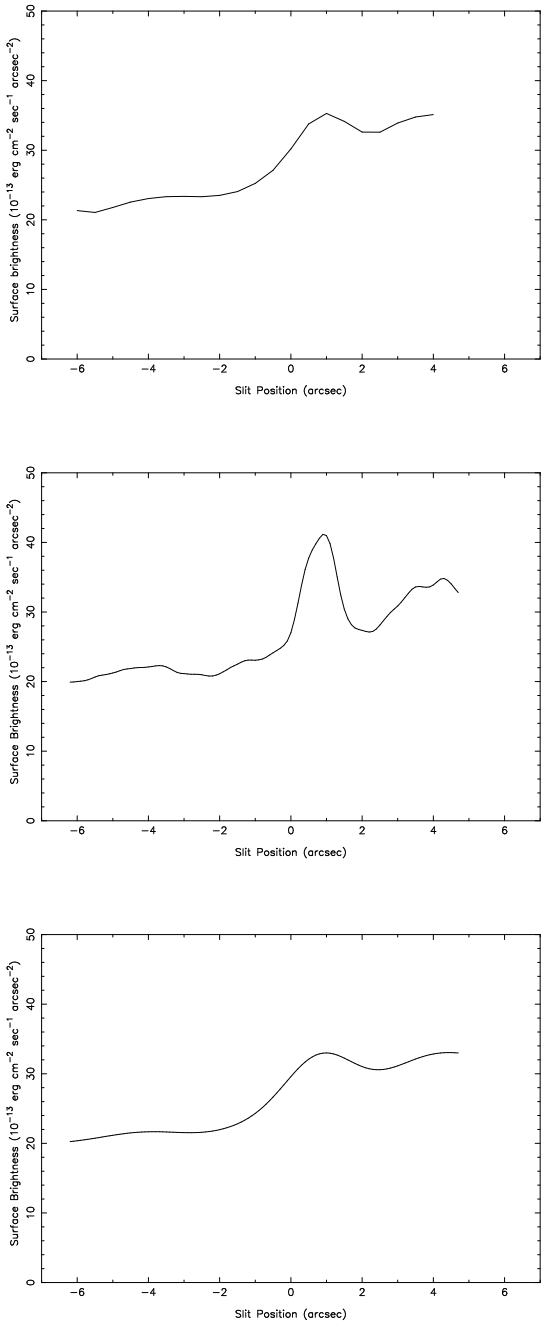

Fig. 3.— Hα region comparison between ground-based echelle spectroscopy (top) and WFPC2 photometry (F656N) (middle, bottom) as a function of slit position. The bottom panel is the result of a 2″ Gaussian convolution of the WFPC2 slit extraction (middle) to simulate the 2″ seeing. These include Hα, continuum and line contamination from neighbouring lines (namely, [N II]).

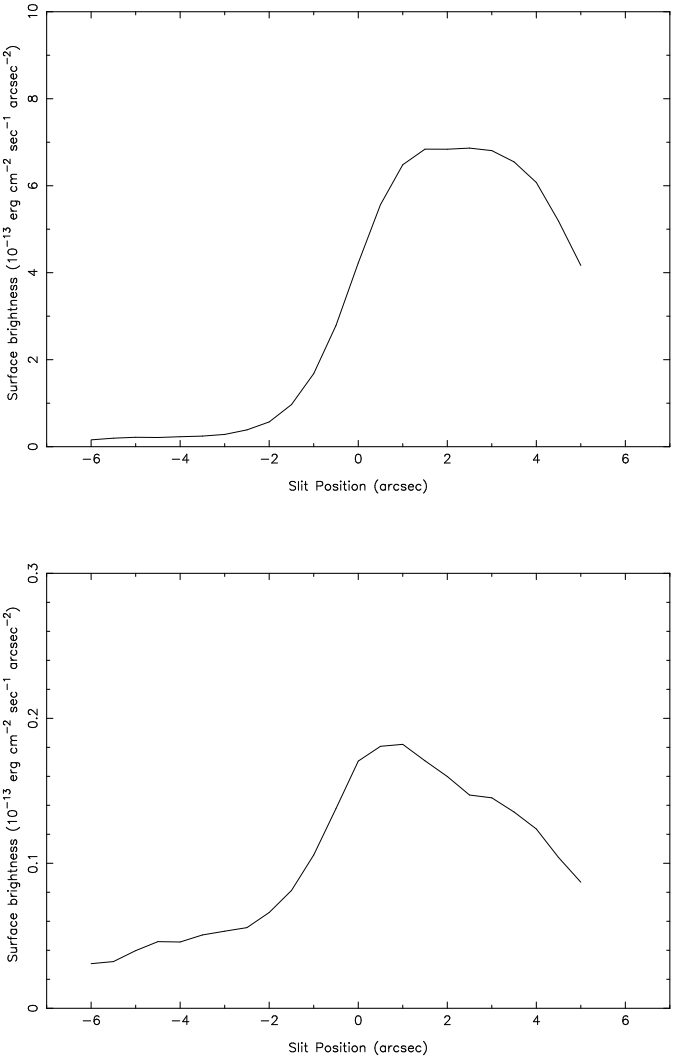

Fig. 4.— Variation of the [O III] 5007 (top) and [O II] 3726 (bottom) velocity-shifted shock component line flux across the 12.5″ slit (25 pixels). The greater O+/O++ ratio near the eastern, leading edge, indicates a somewhat higher density there.

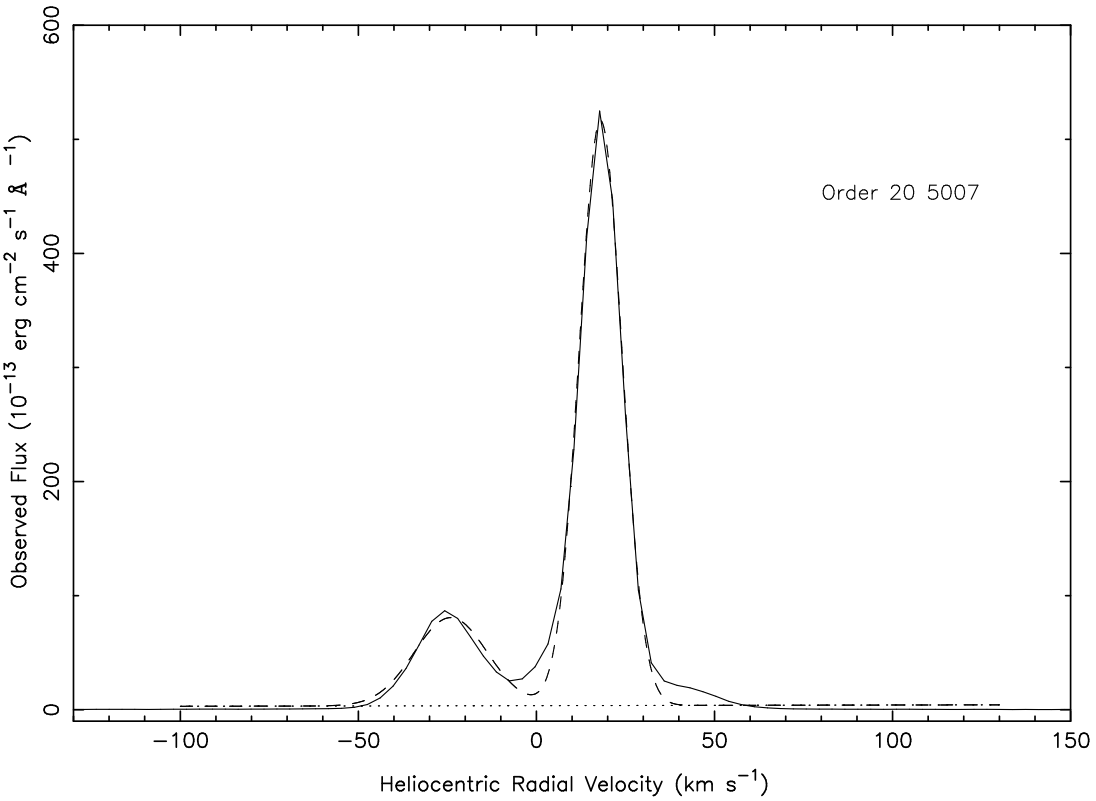

Fig. 5.— Double Gaussian fit of the nebular and velocity-shifted shock components. Eight parameters were used in the fit: FWHM, peak wavelength and area for both components, and two parameters to fit the continuum baseline level and slope. There is a third scattered light (red-shifted) component which was not fit, explaining the poor fit redward of the nebular component. The uncertainties quoted in Table 2 reflect this poor fit. The systemic (nebular) heliocentric velocity is $+18 \pm 2$ km s^{-1} for [O III] (O'Dell 2001b).

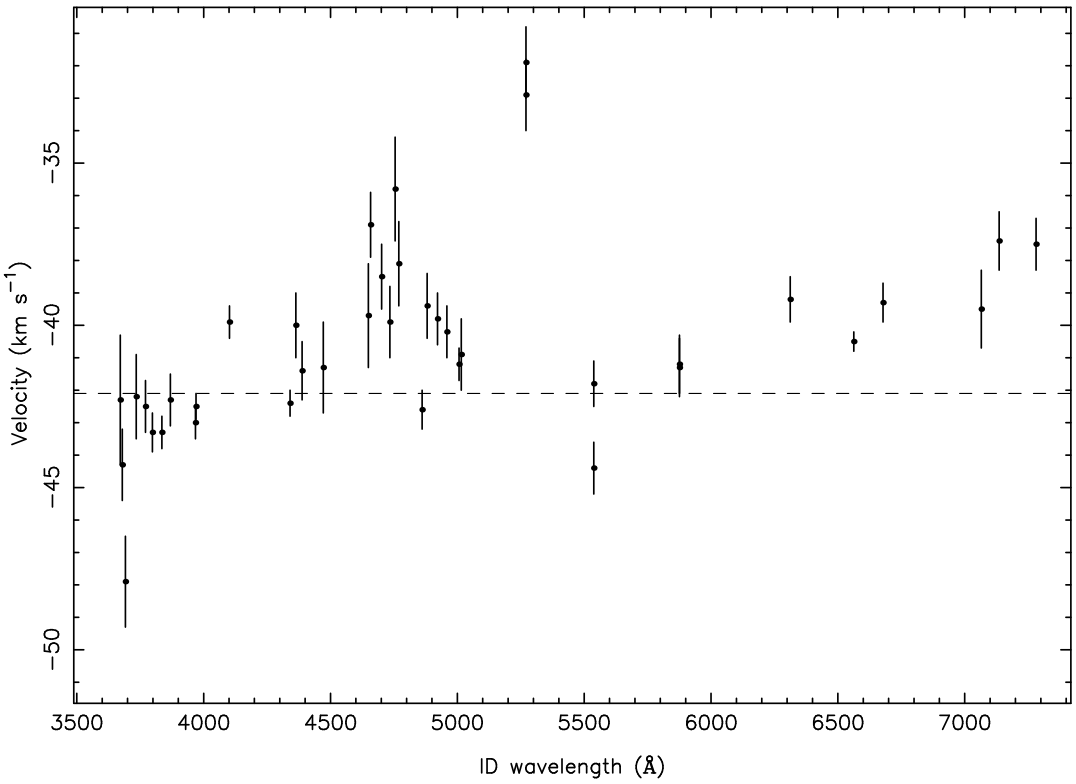

Fig. 6.— Measured velocity of shock component (with respect to nebular H I recombination lines) for high S/N ($S/N > 5.2$) lines from unconstrained double Gaussian fit with 1σ confidence interval determined from the fit. Constrained double Gaussian velocities (-42.1 km s^{-1}) are not plotted individually, but are represented by the horizontal dashed line. The anomalous [Fe III] 5270.4 velocity is discussed in § 3.1.

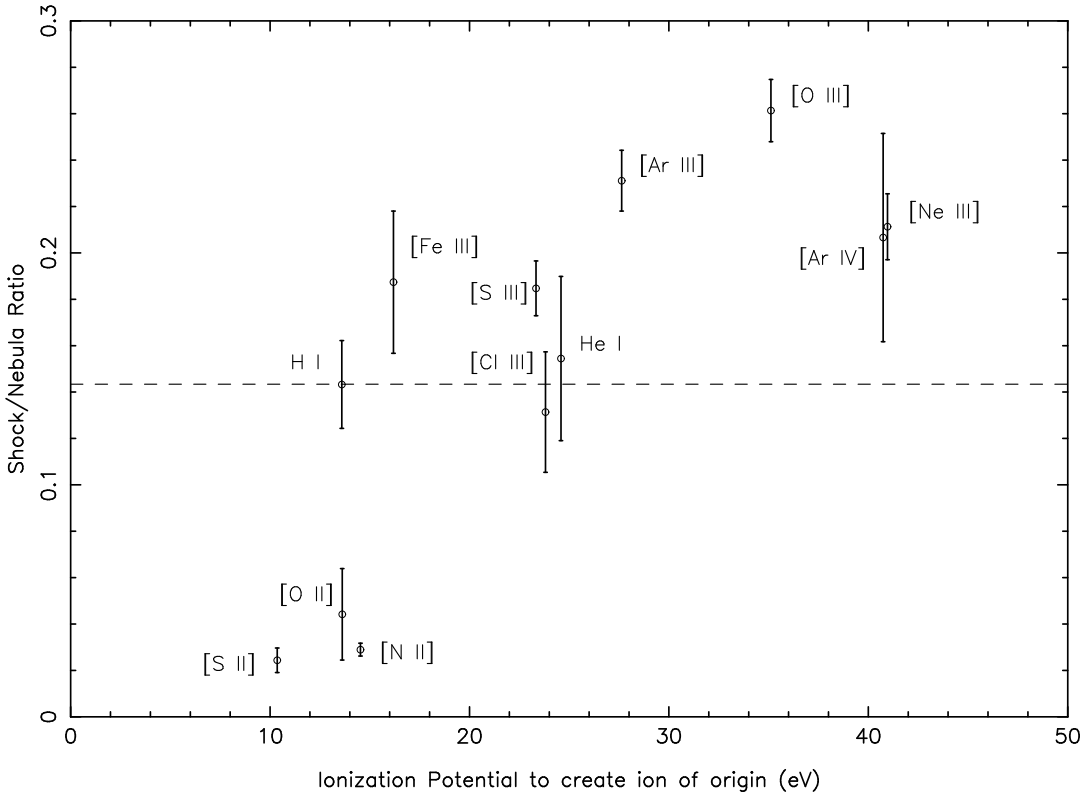

Fig. 7.— Weighted average of shock-to-nebula line ratios (with 1σ error bars) from Column (9) of Table 1 as a function of the ionization potential needed to create the associated originating ion. The ionization potential serves to differentiate ions with different ionization fractions while the shock-to-nebula ratio is a measure of the optical thickness of the shock to ionizing radiation. If the shock were optically thick, this ratio would be close to one for all lines. H I is presented as a standard for shock/nebula ionization comparison as its originating ion (H^+) has an ionization fraction of roughly one throughout both the shock and the nebula. The ratios of the medium-ionization species ([O III], [Ar III], [Ne III]) all lie above H I as their ionization fractions (averaged through the model) are higher in the shock than in the nebula. Conversely, the ratios of the low-ionization species ([O II], [N II], [S II]) lie below H I.

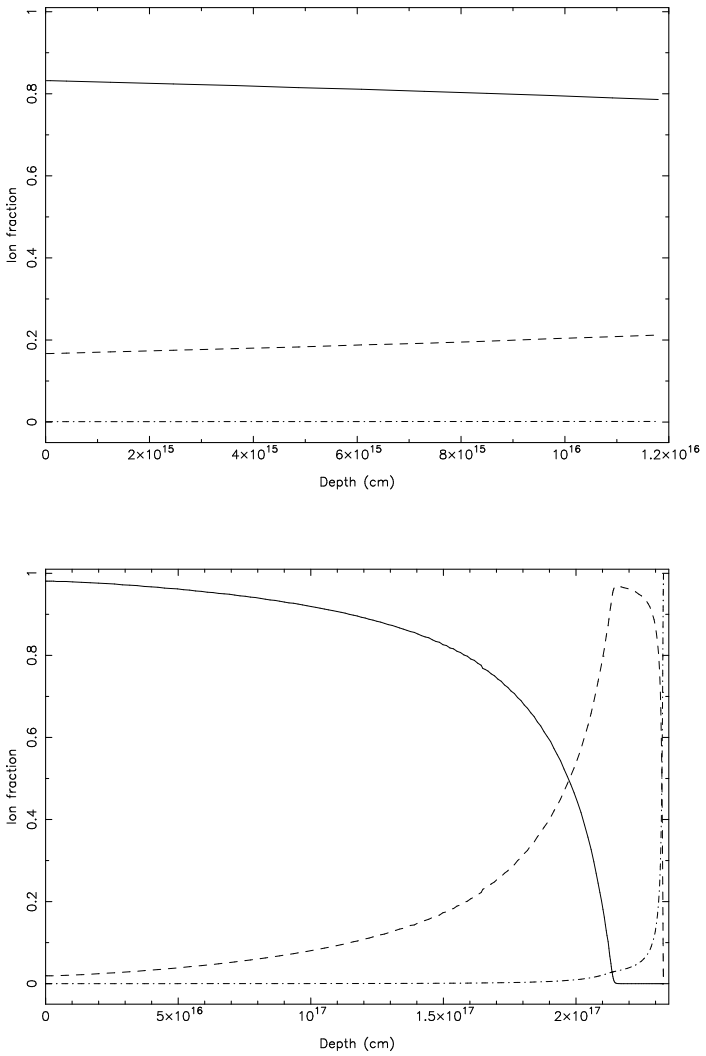

Fig. 8.— Ionization fraction of Fe as a function of depth from the x2shock model (top) and from the nebular model (below) Fe^{+++} ——; Fe^{++} - - - - ; Fe^{+} -·-·-·- . These structure differences lead to differences between shock-to-nebula ratios for low- and medium-ionization species as shown in Fig 7.